Ecological Indicators 154 (2023) 110639

Contents lists available at ScienceDirect

Ecological Indicators

journal homepage: www.elsevier.com/locate/ecolind

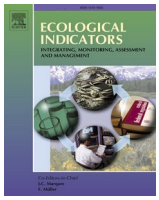

Assessing a multi-method approach for dryland soil salinization with respect to climate change and global warming – The example of the Bajestan region (NE Iran)

Azra Khosravichenar [a,b,*,1], Mehdi Aalijahan [c,d,1], Saeid Moaazeni [e], Anthony R. Lupo [f], Alireza Karimi [g], Mathias Ulrich [a,h], Naser Parvian [i], Aboozar Sadeghi [d], Hans von Suchodoletz [a,1]

[a] Institute of Geography, Leipzig University, 04103 Leipzig, Germany
[b] Institute of Geography, Technische Universität Dresden, 01069 Dresden, Germany
[c] Faculty of Human and Social Sciences, Geography Department, Marmara University, Istanbul 34722, Turkey
[d] Department of Physical Geography, Mohaghegh Ardabili University, Ardabil 5619911367, Iran
[e] Department of Rehabilitation of Mountain and Arid Zone, Faculty of Agriculture and Natural Resources, University of Tehran, Iran
[f] School of Natural Resources, University of Missouri, Columbia, MO 65202, USA
[g] Department of Soil Science, Faculty of Agriculture, Ferdowsi University of Mashhad, Mashhad 9177948978, Iran
[h] German Federal Environment Agency, Dessau, Germany
[i] Faculty of Natural Resources and Environment, Ferdowsi University of Mashhad, Mashhad, Iran

ARTICLE INFO

Keywords:
Desertification
Drylands
Iran
Playa
Regional and global climate change
Remote sensing
Soil salinization

ABSTRACT

Dryland soil salinization strongly affects soil properties, with severe consequences for regional ecology, agriculture and the aeolian dust dynamics. Given its climate-sensitivity it forms a serious environmental hazard, and to cope with this challenge during current global warming it needs to be better understood. The Bajestan Playa in the strongly salinization-affected Iranian drylands hosts several protected areas and forms an important regional dust source. Hence, soil salinization in this region affects local and regional ecosystems and societies, but was not systematically studied yet. Using an unprecedented comprehensive approach we systematically monitored regional soil salinity 1992–2021 using remote sensing as well as on-site field and laboratory measurements, and linked these with regional and global climatic data to understand (i) the spatio-temporal soil salinity dynamics, (ii) the impact of regional and global climate changes, and (iii) the potential of our approach for further soil salinity studies.

Our annual time resolution over three decades provided significantly deeper and unprecedented insights into soil salinization: Both regional annual precipitation and temperature control soil salinity, but the latter responds to precipitation with time lags of up to two years and to higher temperatures without any time lag. This probably reflects the transport time of leached soluble salts from their sources following humid years. No systematic soil salinity changes were observed within the playa basin, but outside the basin soil salinity systematically increased. Whereas regional precipitation did not show a systematic trend during the last decades, regional temperature increased and was mostly correlated with the increasing GLOTI, POL and TSA climatic indices. Hence, given ongoing global warming a further increase of regional soil salinization should be expected, with serious consequences for saline dust emissions, the regional protected areas and climate-related migrations. Altogether, our multi-disciplinary pioneer study demonstrates a high future application potential also for other salinity-affected drylands, forming a base to deal with the consequences of ongoing global climate change.

1. Introduction

Drylands (aridity index < 0.65) cover > 40% of the global land surface today, and host > 38% of the world's population (UNEP-WCMC, 2007; Huang et al., 2017). Intensified greenhouse gas emissions, leading to global warming and climate change, augmented the frequency and

* Corresponding author.
E-mail addresses: azra.khosravichenar.2@uni-leipzig.de (A. Khosravichenar), mehdi_alijahan@yahoo.com (M. Aalijahan).
[1] Equal contributions to the preparation of this manuscript.

https://doi.org/10.1016/j.ecolind.2023.110639
Received 7 April 2023; Received in revised form 16 June 2023; Accepted 6 July 2023
Available online 10 July 2023

severity of extreme climate events and environmental challenges worldwide. This holds especially true for ecologically sensitive drylands, making them especially vulnerable towards these changes (Kweku et al., 2018; Aalijahan et al., 2019; Aalijahan et al., 2022; Nama et al., 2022). Hence, drylands will increase and often become drier during the near future (Feng and Fu, 2013; Huang et al., 2017; Cicek et al., 2022), what will significantly change their hydro-geomorphic and ecological processes with severe consequences for local societies (Ravi et al., 2010; Burrell et al., 2020; Khosravichenar et al., 2020). One fast environmental process in drylands is the soil salinity dynamics, i.e. soil salinization due to surficial accumulation of water-soluble salts. This is caused by an annual rainfall deficit that hinders salt leaching into the subsoil, and strongly affects the physical and chemical soil properties leading to severely changing ecological site conditions (Stockle, 2002; Metternicht and Zinck, 2008). As a consequence, agricultural land use in affected areas is complicated or even rendered impossible (Rengasamy, 2006). Furthermore, such areas are sources of saline aeolian dust affecting larger downwind areas (Ge et al., 2019, Zucca et al., 2021). Hence, soil salinization forms a serious global environmental hazard in the context of the current global climate change (Dehhan and Taylor, 2002; Metternicht and Zinck, 2003; Nawar et al, 2015). Therefore, to plan effective strategies in combatting dryland degradation and to forecast the aeolian dust dynamics, knowledge about regional soil salinization is necessary (Hassani et al., 2020). However, former multi-annual soil salinity studies generally used large and irregular time steps or only short sample periods (e.g. Wu et al., 2014; Scudiero et al., 2015; Dasgupta et al., 2015; Bannari and Al-Ali, 2020; Hassani et al., 2020; Rafik et al., 2022; Ma et al., 2023), hindering a deeper understanding of this environmental process. Furthermore, apart from singular studies suffering from the above-mentioned shortfalls (Bannari and Al-Ali, 2020; Rafik et al., 2022), regional soil salinization was not compared with global climate change.

Playas are intracontinental endorheic dryland basins with a negative water balance for more than half of the year, being characterized by evaporitic sediments. They often contain lakes that are neither dry nor wet > 75% of the time, showing seasonally and interannually strongly varying lake levels (Briere, 2000). Playas deliver ecosystem services such as groundwater recharge, surface water storage and wetland

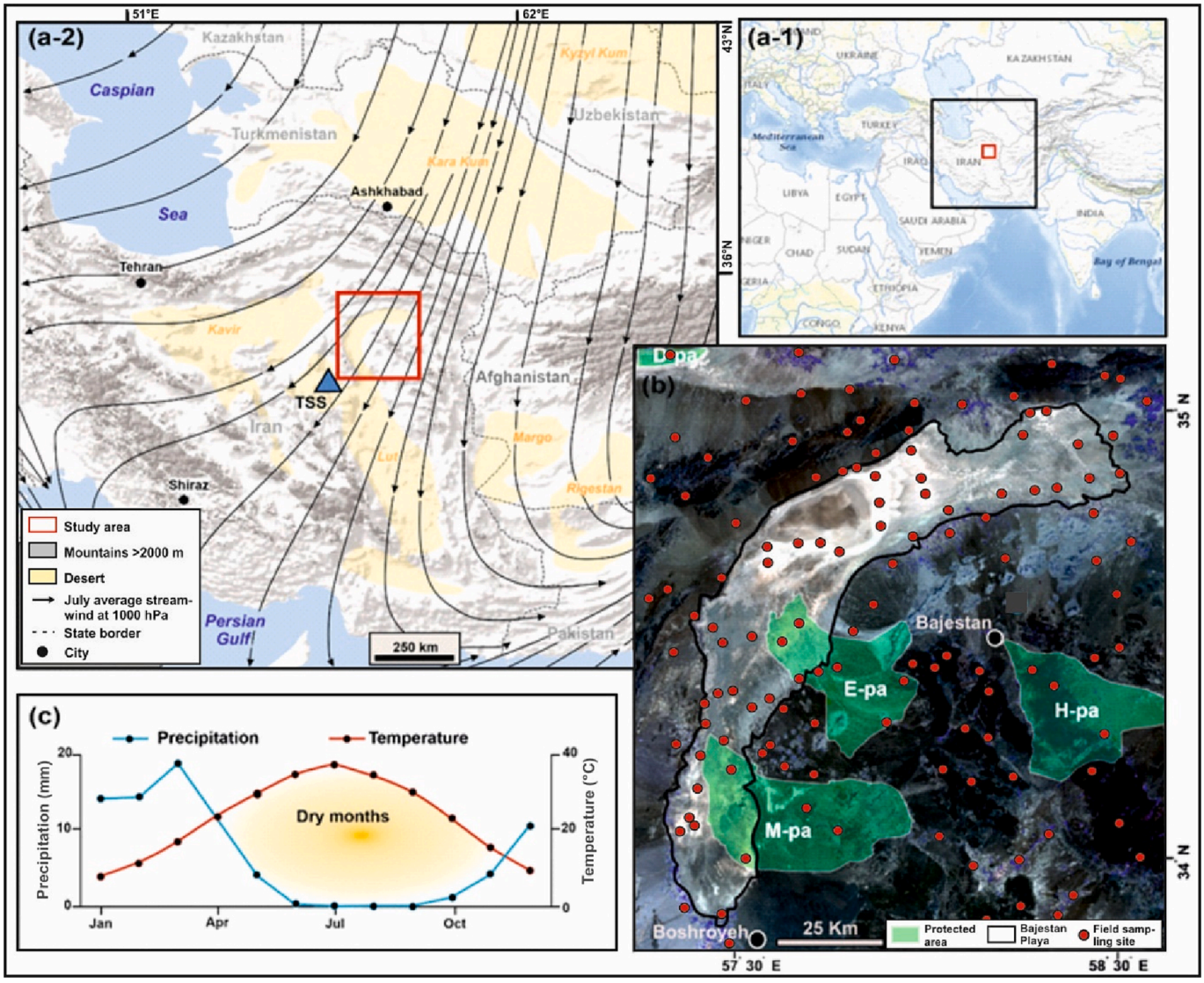

Fig. 1. (a-1): Global overview of the study area (https://earthexplorer.usgs.gov/); (a-2): Location of the study area (red rectangle) in NE Iran (Digital elevation model GTOPO30: https://earthexplorer.usgs.gov), July average stream wind at 1000 hPa (main period of "wind of 120 days": https://psl.noaa.gov/data/gridded/data.ncep.reanalysis.html)(Alizadeh-Choobari et al., 2014), and location of the Tabas synoptic station (TSS: blue circle); (b) Satellite image of the study area (false color composite image of RGB 543 of pan-sharpened Landsat ETM satellite; 08 July 2021).; (c) Climate diagram of the Tabas synoptic station (location see Fig. 1a-2). Protected areas (Fig. b): E-pa = Eftekhari, H-pa = Helali, M−pa = Mozafari, D-pa = Doruneh.

habitats (Bowen and Johnson, 2017). Given the constant accumulation of soluble salts delivered by their tributaries, playas form hotspots of soil salinization (Metternicht and Zinck, 2008). Furthermore, seasonally dry playa surfaces are one main source of saline aeolian dust (Ge et al., 2019, Zucca et al., 2021, Khosravichenar et al., 2021). Caused by the current global climate change and human activities such as irrigation, soil salinization and dust mobilization increased in many playas during the last years, strongly affecting their ecosystem services and regional dust storm intensity (Liu et al., 2015; Bowen and Johnson, 2017; Zucca et al., 2021). Hence, to understand and forecast such processes causing severe consequences for larger areas, soil salinization studies especially in playa regions are necessary.

The extensive Iranian drylands, partly intensively populated today (Guilmoto and Oliveau, 2018), are characterized by an ongoing aridification trend (Sayari et al., 2013; Emadodin et al., 2019). Globally, these drylands are between those being most affected by soil salinization (Hassani et al., 2020). The Bajestan Playa in NE Iran is the second largest playa in this region (Fig. 1a). The playa and its catchment host several protected areas with diverse desert vegetation and wildlife (Sokhanvar et al, 2013; Department of Environment of Iran: https://en.doe.ir) (Fig. 1b). During the dry summer season the playa is influenced by the strong northeasterly "Wind of 120 Days", being linked with dust mobilization. Hence, it forms an important aeolian dust source for inner and southern Iran (Middleton, 1986; Alizadeh-Choobari et al., 2014; Thiam et al, 2021), where the number of climatic refugees increased during the last years (Ebrahimzadeh and Esmaeil Negad, 2017; Mianabadi et al., 2022). However, the soil salinity dynamics of the Bajestan region, significantly influencing local and supra-regional ecosystems and societies, was not systematically studied so far.

We monitored the spatio-temporal soil salinity dynamics in the Bajestan region using a comprehensive approach. Our methodology included a continuous annual remote sensing-based salinity time series spanning from 1992 to 2021, on-site field and laboratory measurements and systematic correlations with regional and global climate parameters. This continuous multi-dimensional approach sets our work apart from previous studies on soil salinity, which predominantly used irregular and/or short time series and hardly linked the soil salinity dynamics with regional and global climate. The goals of this pioneer study were to understand (i) spatio-temporal soil salinity changes in the Bajestan region during the last three decades, and (ii) the impact of regional and global climate changes on these processes, and (iii) the future potential of this comprehensive way to analyse soil salinization with respect to climate change and global warming also for other drylands.

2. Study area

The Bajestan Playa in the drylands of NE Iran, extending between 58°33′ − 58°46′N and 34°58′ − 35°1′E, has a size of ~ 3.725 km^2 and a catchment of ~ 34.170 km^2. The playa surface is very flat, showing an altitude of ~ 760 m a.s.l in the northern central part where a saline playa lake is developed (Fig. 1b).

The playa basin had formed in the northern part of the Lut Block in the eastern part of the Central Eastern Iranian Microplate (Ahmadirouhani et al., 2017). In synchronicity with Quaternary climate changes, lakes had regularly formed within the Bajestan basin and other large topographical basins of Iran, the last phase occurring during the deglaciation around 14 ka. Subsequently, these lakes gradually dried out due to increased Holocene temperatures, forming the current playas (Torshizian and Moosavi Harami, 1999; Ashoori et al., 2005). The southern catchment is dominated by Cretaceous limestones and Mesozoic to Cenozoic igneous rocks, and the northern and western parts by Paleozoic to Cenozoic sedimentary and metamorphic rocks such as slates and phyllites (National Iranian Oil Company, 1957; Ahmadirouhani et al., 2017). The playa basin hosts different kinds of Quaternary deposits, i.e. mostly alluvial fans, dunes and paleolake deposits. The latter, especially found in the central part, are formed by up to several hundred meters thick salt deposits (Behrouzi, 1987; Ashoori et al., 2005). Large parts of the playa surface show extensive salt flats with salt polygons of different sizes. The size of the saline playa lake strongly varies seasonally and inter-annually. Due to the asymmetric catchment area most intermittent streams enter the playa from the northeast and southwest. Only small alluvial fans cover the zone between the northern foot-slopes and the playa basin, whereas a mega-fan extends from the southern shore towards the playa lake (Krinsley, 1970; Ullmann et al., 2019). Next to surficial hard rocks, the region is covered by bare and partly saline desert soils (Dewan and Famouri, 1961).

According to the Köppen-Geiger climate classification the region shows a semiarid to arid steppe climate today (Raziei, 2021), characterized by dry and extremely hot summers and cool winters (Aalijahan and Khosravichenar, 2021). Mean annual precipitation is 77.3 mm, mean annual temperature is 23 °C, and mean annual evaporation is 290.7 mm (https://www.irimo.ir) (Fig. 1c). During summer, the playa is influenced by the northeastern "Wind of 120 Days" linked with regional dust storm activity (Alizadeh-Choobari et al., 2014). During winter westerly disturbances dominate, bringing most of the annual precipitation (Alijani and Harman, 1985).

The region belongs to the Irano-Turanian phytogeographical region (Khosravi et al., 2014; Noroozi et al., 2019). The patchy vegetation is characterized by halophytic species such as *Salsola*, *Salicornicum* and *Atriplex*. Parts of the region host the Eftekhari, Mozarafi, Helali and Doruneh protected areas (Fig. 1b; unpublished map Department of Environment of Iran). Small agricultural fields (pomegranate, saffron, pistachio) are concentrated in the surroundings of the regional settlements.

3. Data and methods

3.1. Remote sensing

3.1.1. Analysis and calculation of salinity indices

To analyze regional soil salinity in the study area encompassing parts of the Bajestan region (17909.5 km^2), we used remote sensing (RS) data between 1992 and 2021 (in the following "RS-study period"). These were taken from Landsat 5 Thematic Mapper (1992–2001), Landsat 7 Enhanced Thematic Mapper Plus (2002–2012) and Landsat 8 OLI sensors (2013–2021) (https://earthexplorer.usgs.gov; row 36, path 160). In accordance to our field campaign in 2021, we only used images from the first week of July. The dry summer season is ideal to detect soil salinity by RS, since low soil moisture causes surficial salt precipitation being easily detectable by well-developed topographical features, such as efflorescence, crusts, puffy structures and cracks (Metternicht and Zinck, 2003; Stavi et al, 2021). The data were pre-processed by radiometric, atmospheric and spectral normalization using ENVI 5.3 software. Soil salinity was calculated by applying ten different salinity indices using combinations of the blue, green, red and/or the near infrared RS-bands (subsequently called "EC-Pred" *[= predicted]*) (see Supplementary Table ST-1), applying the TerrSet geospatial monitoring and modeling software (https://clarklabs.org/terrset).

3.1.2. Calculation of wet-/water-covered and vegetated areas

We used widely applied spectral RS-indices and coding in Google Earth Engine to identify fluctuating wet/water-covered and vegetated areas that are known to influence soil salinization processes (Hou and Rusuli, 2022; Perri et al., 2018): Wet/water-covered surfaces during February and March were calculated using the modified Normalized Difference Water Index (mNDWI) (equation (1) (Feyisa et al., 2014; Szabó et al., 2016; Wang et al., 2020). The vegetation cover for July was calculated using the Normalized Difference Vegetation Index (NDVI) (equation 2), being closely related to green and healthy vegetation showing values > 0.2 (Tucker, 1979; Benedict and Jaelani, 2021; Cetin et al., 2022; Zeren Cetin et al., 2023).

$$mNDWI = \frac{Green - Swir}{Green + Swir} \quad (1)$$

$$\mathrm{NDVI} = \frac{NIR - Red}{NIR + Red} \quad (2)$$

(Swir = shortwave infrared bands, NIR = near-infrared band of Landsat images).

The mNDWI values correspond to: 1–0.2 = water, 0.2–0.0 = humid surfaces, 0.0 - (–0.3) = moderate dry, non-aqueous surfaces, (–0.3) - (–1) = dry, non-aqueous surfaces. The NDVI values range between 1 (very lush vegetation) to –1 (water), with values around 0 corresponding to rock or soil.

3.2. Field work and laboratory analysis

We collected 70 surficial soil samples from 10 * 10 m plots during the first half of July 2021. To obtain representative samples not affected by random effects, five sub-samples were collected from the corners and the center of each plot and mixed into one sample. The geographic positions were determined from the plot center using a hand-held GPS. To representatively encompass the geomorphic-environmental diversity of the study area, the sampling locations were based on remote sensing-derived soil salinity (see chapter 3.3) as well as on topographic and geomorphological features (Fig. 1b).

Electrical Conductivity (EC), an indicator of soil salinity, was measured in the laboratory of the Ferdowsi University of Mashhad (Iran) following Shaw (1994) (subsequently called "EC-Lab" *[= measured in laboratory]*).

3.3. Statistical soil salinity analysis

To construct a robust soil salinity detection model, the ten RS-derived salinity indices (EC-Pred) (chapter 3.1.1) were calibrated with the field-based soil salinity (EC-Lab) (chapter 3.2) using a linear regression model. Root mean squares were used to indicate the inequality of variance and correlation of that model. Given that salinity index SI (Khan et al. 2005) yielded the best agreement between EC-Pred and EC-Lab ($R^2 = 0.896$; see supplementary Table ST-1), this index was used to categorize six different soil salinity classes according to Jenks Natural Break Algorithm that is based on natural groupings inherent in the data and minimizes the variance within and maximizes the deviations between the classes (Chen et al, 2013; Stavi et al., 2021, and citations therein). Based on these soil salinity classes, we used the Land Change Modeler for Ecological Sustainability (LCM) to detect spatio-temporal soil salinity changes within the study area over the RS-study period (https://clarklabs.org; Eastman and He, 2020).

3.4. Climatic analysis

To analyse possible climatic influences on the regional soil salinity dynamics, we used annual averages of daily resolved local temperature and precipitation data from the nearby Tabas synoptic station (Fig. 1a) between 1961 and 2021 (hereafter referred to as "climatic time scale"; see supplementary Table ST-2). The longer time scale of the climatic analyses (61 years) compared with the shorter RS-study period (30 years) allows to better evaluate the robustness of observed climatic trends. Furthermore, to understand the impact of global climatic factors on the climate of the Bajestan region, we compared 37 global climate indices with regional climatic parameters by applying Pearson correlation analyses (source: https://psl.noaa.gov/data/climateindices/list; for the MJO [Madden-Julian Oscillation] Index see: https://www.cpc.ncep.noaa.gov/products/precip/CWlink/MJO/mjo.shtml). The statistical methods are described below.

3.4.1. Regression analysis

Simple linear regression was applied to establish the relationship between two variables using a straight line being closest to the data, by determining slope and intercept and minimizing the regression error.

Furthermore, we applied sixth-order polynomial regression to analyze nonlinear relationships between an independent variable × and a dependent variable y in the form of E(y|x) (Montgomery et al., 2021).

3.4.2. Cross correlation

Cross correlation was used to examine possible relationships between regional climate parameters, the water-covered/wet area during February/March, and NDVI and soil salinity during July for the RS-study period 1992–2021. This allowed to determine the time lags of their best agreement for periods of up to 4 years (Menke and Menke, 2016; Begum et al., 2021). The basic equations are given below in equation (3) and (4) (Oktaviani and Setiawan, 2021):

$$r(L) = \frac{\sum_{k=0}^{N-L-1}(x_{(k+L)} - mx)(y_k - my)}{\sqrt{\left[\sum_{k=1}^{N-1}(x_k - mx)^2\right]\left[\sum_{k=0}^{N-1}(y_k - my)\right]}} \quad L \geq 0 \quad (3)$$

$$r(L) = \frac{\sum_{k=0}^{N-|L|-1}(x_k - mx)(y_{(k+|L|)} - my)}{\sqrt{\left[\sum_{k=0}^{N-1}(x_k - mx)^2\right]\left[\sum_{k=0}^{N-1}(y_k - my)\right]}} \quad L < 0 \quad (4)$$

(mx = average rows of data on variable ×, my = average rows of data on variable y, r = cross-correlation value, d = time of highest correlation between the two variables, L = time lag).

3.4.3. Mann-Kendall test

Nonparametric statistics, being much less affected by outliers and other abnormalities (Lanzante, 1996), provides a measure of monotonic linear dependence (Davis & Sampson, 1986; Rossi et al., 1992). The most commonly used nonparametric test for trends in environmental variables is the Mann-Kendall test (MK) (Yadav et al., 2014; Pohlert, 2016; Aalijahan et al., 2023). This test does not require a specific data distribution, and can be used to analyze change trends, break points and abrupt changes within time series (Ye et al., 2013; Sung et al., 2017; Zhang et al., 2018). Hence, it was used for both the long climatic time scale 1961–2021 and the short RS-study period 1992–2021 to examine significant points of regional climate change.

For an assumed data series K ($k_1, k_2, \cdots k_n$), n is the length of the data series. First, the cumulative statistic parameter S_k, being the cumulative number of values at time i being greater than at time j, is calculated (equations (5) and (6):

$$S_k = \sum_{i=1}^{k} r_i \quad k = 2, 3, \cdots n \quad (5)$$

$$r_i = \begin{cases} 1 x_i > x_j \\ 0 x_i \leq x_j \end{cases} \quad j = 1, 2, \cdots i-1 \quad (6)$$

Subsequently, assuming random independence of the time series, the statistic parameter U'I is defined as follows (equation (7):

$$U'I = \frac{S_k - E(S_k)}{\sqrt{Var(S_k)}} \quad k = 1, 2, \cdots, n \quad (7)$$

U'I = 0, and $E(S_k)$ and $Var(S_k)$ represent expected value and variance of the cumulative value S_k, respectively:

$$E(S_k) = \frac{k(k-1)}{4} \quad (8)$$

$$Var(S_k) = \frac{k(k-1)(2k-5)}{72} \quad (9)$$

U'I is a standard normal distribution, i.e. a statistical sequence computed from the sequence of time series X. At a significance level α, $|U'I| > U_\alpha$ indicates an apparent trend change within the time series.

Using the inverse time series, we calculated U'I again applying the calculation procedure described above, where UI = -U'I and k = n,n −1,⋯,1 (Liu et al., 2020).

4. Results

4.1. Soil salinity dynamics

The calibration of RS-derived salinity index SI (EC-pred) with field-derived soil salinity (EC-Lab) resulted in six different soil salinity classes between non-saline to extreme salinity (Table 1; exemplary photos with typical features of the six classes please see in supplementary Figure SF-1). During the studied month of July no open water areas existed in the study area, hence no separate class was designated for it.

Table 1 presents the salinity values of each soil salinity class in the study area, their spatial share during the first (1992–2001) and last studied decade (2012–2021), geomorphic position, specific surface properties and vegetation cover. Generally, outside the playa basin mostly the non-saline, low, moderate and high classes are found, whereas inside the playa basin the high, very high and extreme classes dominate (Fig. 2).

Figs. 2 and 3 illustrate the spatio-temporal dynamics of the soil salinity classes. The very high and high classes showed continuously increasing trends throughout the RS-study period, whereas the low class continuously decreased. In contrast, the moderate class hardly showed any systematic change. Also the non-saline and extreme classes did not systematically change during most of the time, however, their areas strongly increased in 2021. Fig. 4 shows area changes between these classes during the three studied decades. In particular, outside the playa basin moderate saline areas went over to the high and very high classes during the first and third studied decades, whereas within the playa basin extreme saline areas passed over to the high and very high classes throughout the complete study period (Fig. 4a). The changes of different classes to the extreme class are shown in Fig. 4b. Obviously, this happens primarily for areas within the playa basin that were originally classified as the very high, high and moderate classes. The latter two contributed particularly during the third studied decade. The extent of the wet/water-covered area within the playa basin in February/March showed erratic fluctuations during the RS-study period, and was mainly confined to the areas of extreme and very high (summer) soil salinity.

The NDVI was used to analyse vegetation changes during the RS-study period. Fig. 5a shows the vegetation distribution exemplarily for 1992. Most vegetation is found on areas of low soil salinity (34.2%), closely followed by the non-saline (33.6%), moderate (30.0%), high (7.7%), very high (0.6%) and extreme (0.0%) classes. For the entire RS-study period fluctuations in vegetation density over several years are visible, and extraordinary peaks were reached in 2019 and 2020 (Fig. 5b). However, the average vegetation distribution remained the same over almost the entire study period.

4.2. Temporal evolution of regional annual precipitation and temperature

Mean annual precipitation did not show a clear trend for the long climatic time scale 1961–2020. However, linear and 6th order polynomial regression for the shorter RS-study period 1992 – 2021 show a decrease especially from 2004 until 2016 (Fig. 6). At the end of the RS-study period a short three-year wet period occurred 2018–2020, but in 2021 precipitation dropped again.

Mean, maximum and minimum annual temperature linearly increased since 1961 (Fig. 7). However, on the long climatic time scale the increase of minimum annual temperature, being especially strong during the 1970 s and 1980 s, was much higher (linear regression slope a = 0.094 °C) than for mean and maximum annual temperature (each a = 0.018 °C). In contrast, for the shorter RS-study period the slope of the increase of maximum annual temperature (a = 0.069 °C) was higher than for average (a = 0.060 °C) and especially minimum (a = 0.037 °C) annual temperature. Also 6th order polynomial regression, recognizing periodic trends of the temperature parameters, confirms the increasing trends for both time scales.

4.3. Mann Kendall trend analysis

The Mann-Kendall trend analysis of mean annual precipitation on the longer climatic time scale did not show a significant trend, since the significance level of ± 1.96% was hardly exceeded despite some intersections between the UI and U'I lines. However, on the shorter time scale of the RS-study period the 2009 intersection is significant, forming a sudden downward change point of precipitation (Fig. 8a).

Maximum and mean annual temperature indicate long-term downward trends during the first years of the longer climatic time scale (Fig. 8b, c), followed by strong upward trends lasting until today. However, the intersections of these temperature variables during their

Table 1
Characteristics and surface area of the six soil salinity classes.

Soil salinity class	Thresholds of Natural Break values (Jenks)	EC-Lab values *[dS m^{-1}]*	Spatial proportions *[%]* (1992 – 2001 / 2012–2021)	Geomorphic position	Surface properties	Vegetation cover
Non-saline	0–4.3	0–4	8.9 / 8.1	Rock outcrops and nearby elevated areas such as uppermost parts of alluvial fans, higher banks of drainage channels	Hardly salt-covered	Agricultural lands with traditional irrigation systems growing drought-resistant plants such as pistachio; riparian vegetation along rivers
Low	4.3–14.5	4–10	32.6 / 26.2	Upper parts of alluvial fans, abandoned farmlands, bajadas	Occasional salt stains/crystals	Halophytic plants
Moderate	14.5–24.7	10–20	27.6 / 27.7	Middle parts of alluvial fans, bajadas	Occasional salt stains/crystals	Halophytic plants
High	24.7–36.4	20–40	16.0 / 20.1	Highest parts of the lowlands including slightly elevated alluvial fan surfaces	White-brown salt-encrusted flowery or puffy surfaces of medium intensity with vertical microrelief of 10–20 cm; seasonally cemented	At alluvial fan surfaces bordering areas of medium salinity 2–3 species of highly salt-tolerant plants
Very high	36.4–52.15	40–60	9.9 / 12.8	Lowlands and lowest parts of alluvial fan surfaces	Intensive white-brown salt-encrusted flowery or puffy surfaces with vertical microrelief of 10–20 cm; seasonally cemented	No
Extreme	>52.15	>60	5.0 / 5.0	Mostly flat dried lake bed in central playa basin	Pure salt crusts, temporally inundated during winter, some years swampy during summer	No

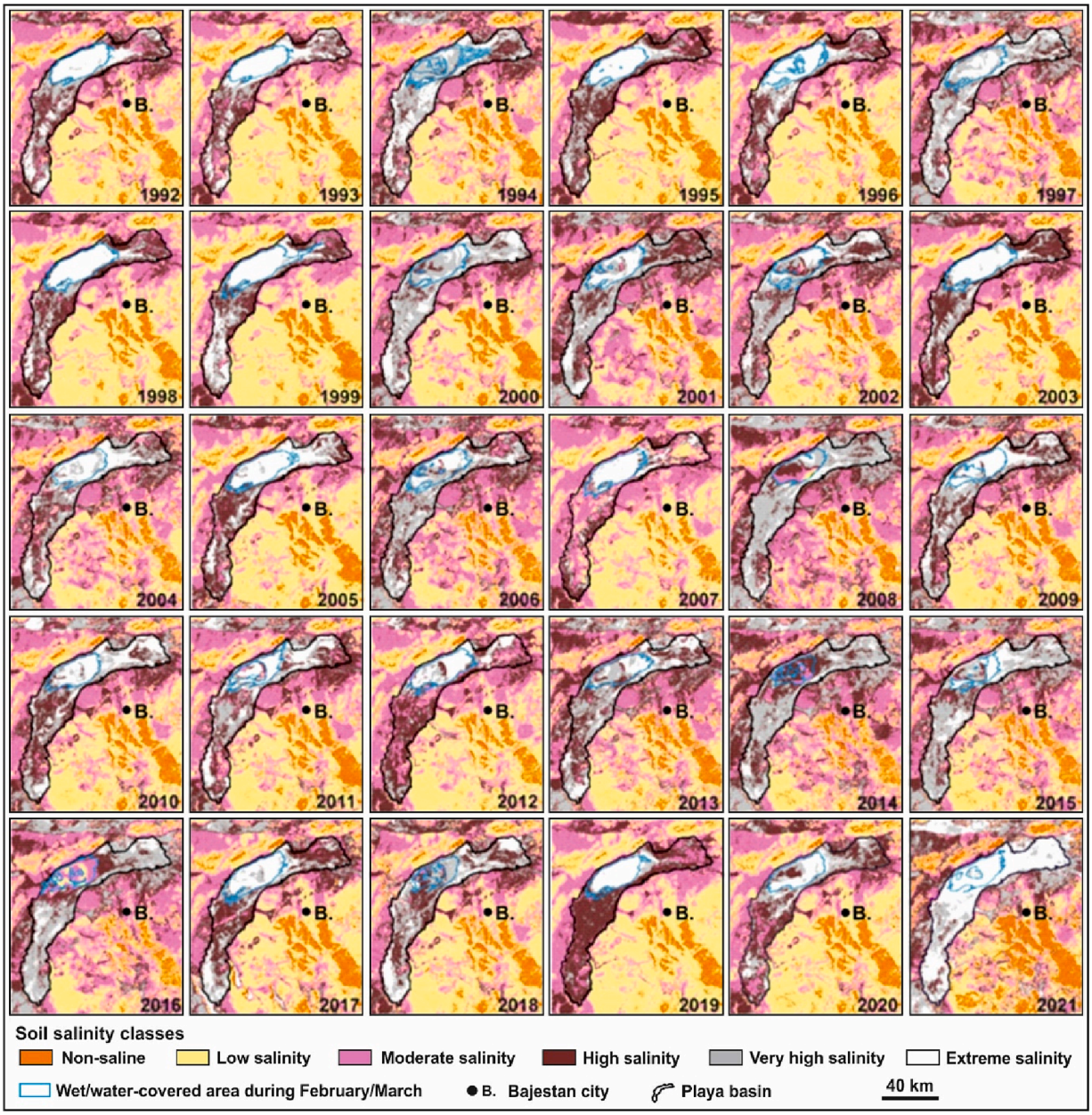

Fig. 2. Maps of the annual distribution of the six RS-derived soil salinity classes and the wet/water-covered area in the study area between 1992 and 2021. The corresponding values of each class and year can be found in Supplementary Table ST-3).

upward trends are not significant (Fig. 8b, c). In contrast, the upward trend of minimum annual temperature started much earlier, and the intersection in 1988 forms a sudden upward change point of this parameter (Fig. 8d). On the shorter time scale of the RS-study period all three temperature variables show upwards trends, and consecutive intersections occurred in the time series of all these variables. For mean and maximum annual temperature the intersections in 2007 and 2012 suggest significant trend changes (Fig. 8b, c), as well as the intersections of minimum annual temperature in 1996 and 2008 (Fig. 8d).

The regional temperature variables correspond well with the global temperature increase (Fig. 8e), what holds especially true for the shorter RS-study period. The global temperature increase intensified since ca. 1992, possibly causing the strong upward trends of maximum and mean annual temperature since that time. Interestingly, minimum annual temperature highly corresponded to the global temperature rise already since 1975, i.e. much earlier than the other parameters.

4.4. Influence of regional climate changes and the wet/water-covered area in the playa basin on soil salinity, and the role of regional vegetation

To depict the influence of regional climate changes on soil salinity in the Bajestan region, we cross-correlated regional climate parameters with soil salinity (see supplementary Table ST-4; Fig. 9). Furthermore, to understand a possible influence of the wet/water-covered area in the playa basin during February/March on summer soil salinity, we cross-correlated its extent with the extreme soil salinity class being dominant within the basin. These cross-correlations were calculated for time lags (delays) of up to 4 years. Negative lags indicate a lead of the climatic parameters and of the wet/water-covered area extent, whereas zero time lags indicate a simultaneous reaction of soil salinity to these factors. Furthermore, soil salinity was also correlated with the NDVI, and given the strong influence of regional climate on dryland vegetation density the NDVI was also correlated with mean annual precipitation and temperature.

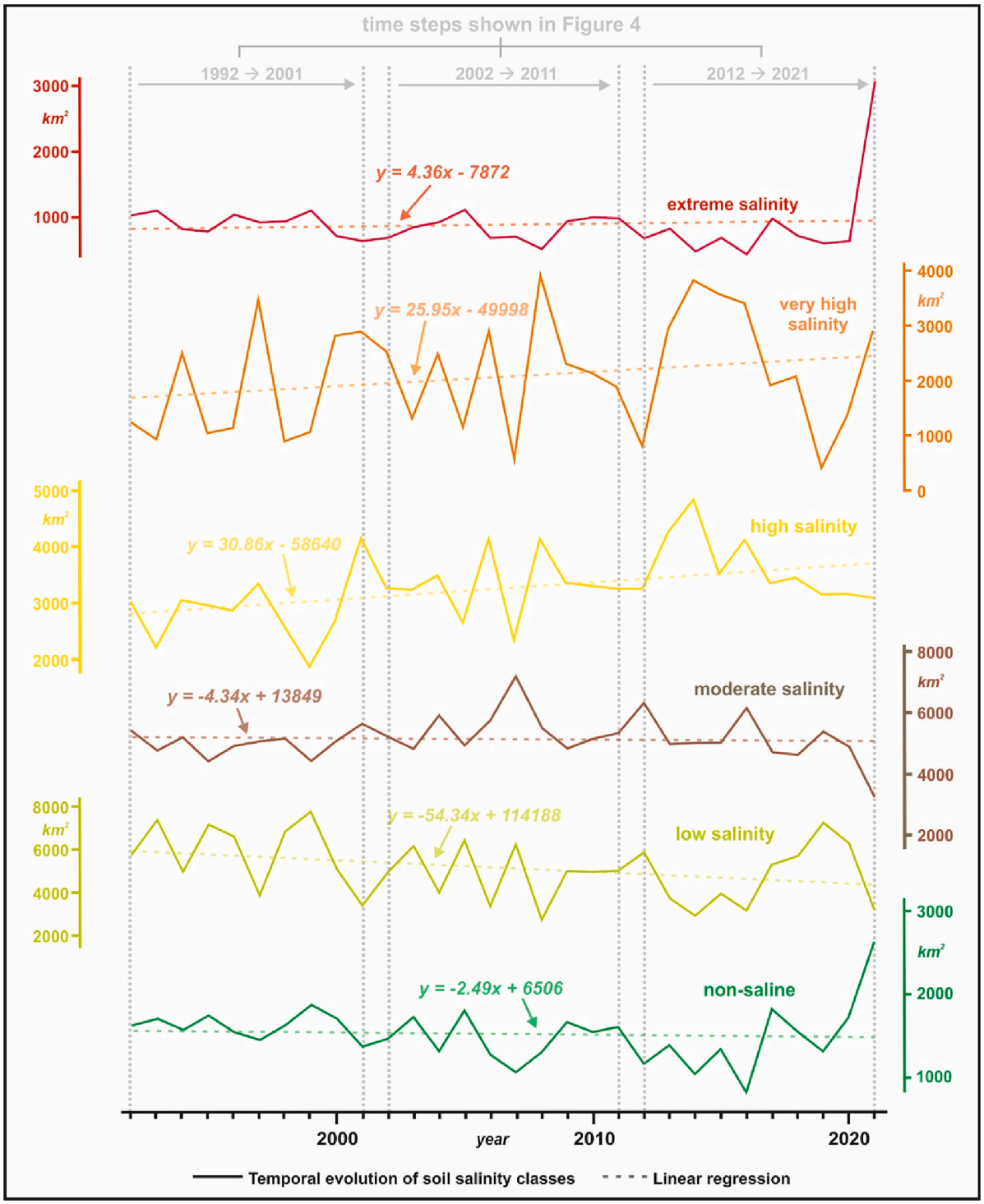

Fig. 3. Total area changes of the six soil salinity classes during the RS-study period 1992–2021.

We observe a significant positive correlation (r = 0.604) between soil salinity and regional annual precipitation for a time lag of two years, and a significant negative correlation (r = -0.473) for a time lag of one year (Fig. 9a). Maximum and mean annual temperature showed the largest significant positive correlations with soil salinity for a time lag of zero, with r-values of 0.609 and of 0.482, respectively. In contrast, minimum annual temperature showed a significant negative correlation (r = -0.433) with a time lag of one year (Fig. 9b-d). The correlation between the wet/water-covered area in the playa basin during February/March and extreme soil salinity in July did not show any significant correlation (Fig. 9e). The correlation of the NDVI with mean annual precipitation and temperature showed a very slight significant positive correlation of r = 0.373 and a significant negative correlation of r = -0.493, respectively, both with time lags of zero. The positive correlation of NDVI with mean annual precipitation was possibly caused by the strong vegetation increase 2019 – 2020 during an extraordinarily wet period. Finally, the correlation of NDVI with the low soil salinity class showed a significant positive correlation of r = 0.619 with a time lag of zero. No significant correlation was found between NDVI and the non-saline class (Fig. 9f-i).

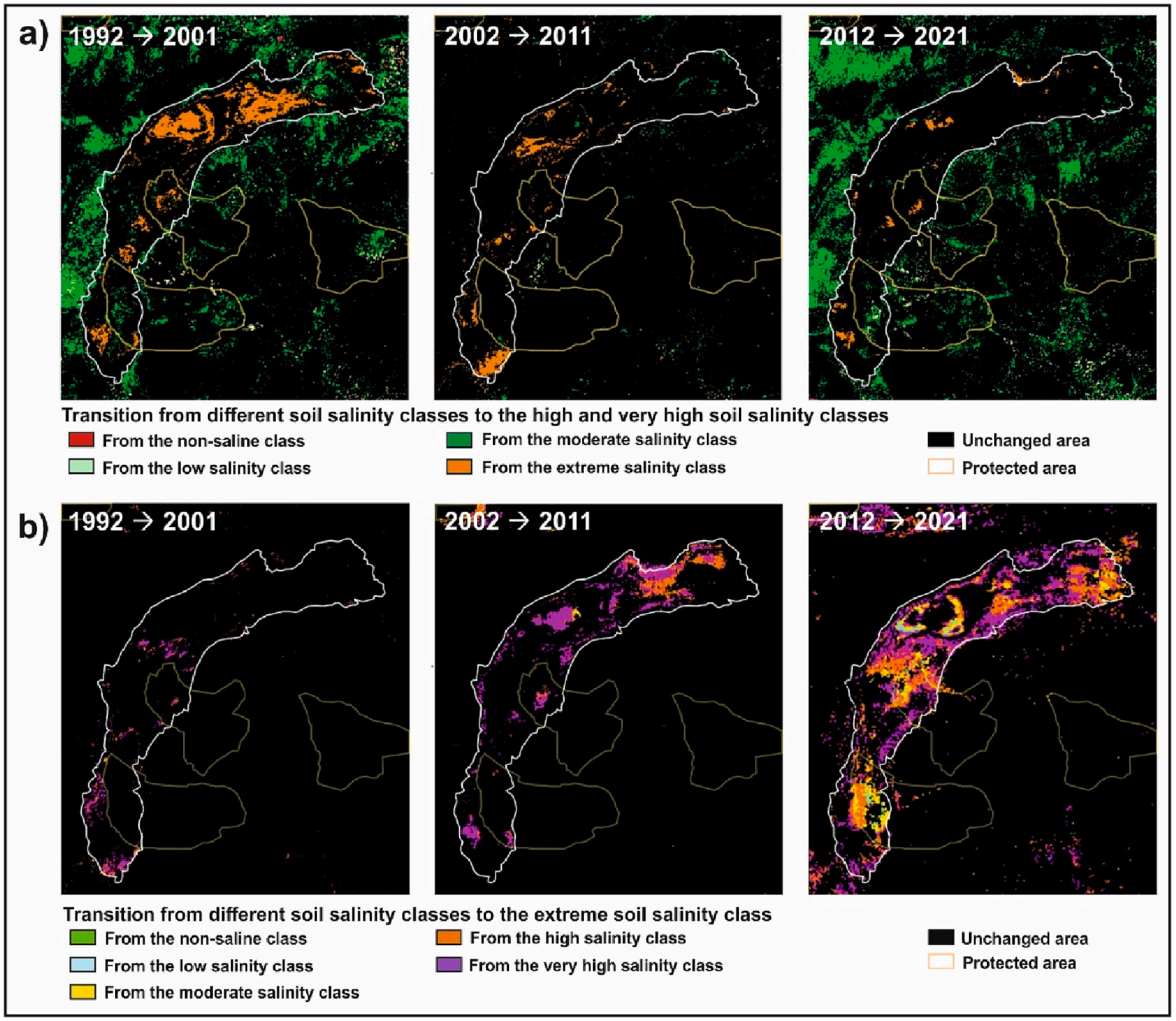

Fig. 4. Maps showing changes between the soil salinity classes for the three studied decades by comparing 1992 with 2001, 2002 with 2011, and 2011 with 2021 (calculated by Land Change Modeler for Ecological Sustainability). (a) Changes from different classes to the merged high and very classes, (b) Changes from different classes to the extreme class.

4.5. Teleconnection analysis

The correlations between global climatic indices and climatic parameters in the study area are shown in Table 2.

Out of the 35 regarded teleconnection indices only some sub-indices of the Madden–Julian Oscillation (MJO) Index show significant negative correlations with mean annual precipitation in the Bajestan region, i.e. sub-indices 9, 10, 1 and 2 (the MJO indices at 20, 70, 80 and 100°eastern longitude) (Table 2). Between those MJO - E70 Index 10 shows the highest negative correlation (r = -0.482, confidence level 0.99%). Also on a short multi-annual periodic time scale, expressed by 6th order polynomial regression, this negative correlation is well recognizable despite a missing long-term trend (Fig. 10a).

Nine out of the 35 global teleconnection indices, and the Global Land-Ocean Temperature Anomaly Index (GLOTI), show significant correlations with regional temperature (6 positive and 4 negative, respectively) (Table 2). Mean annual temperature shows the highest number of significant correlations, followed by maximum and minimum annual temperature. All regional temperature parameters, and especially mean and maximum annual temperature, show significant positive correlations with GLOTI that all show long-term upward trends. They also positively correlate on a multi-annual time scale, as is demonstrated by the 6th order polynomial regression of mean annual temperature and GLOTI (Fig. 10b). Hence, the increasing GLOTI Index obviously strongly controls the temperature increase in the Bajestan region.

Among the correlated teleconnection indices, POL and TSA show the most negative and positive effects on regional temperature. The annual temperature parameters and POL show negative correlations (Table 2), and according to 6th order polynomial regression these opposite trends also hold on a short multi-annual periodic time scale (see Fig. 10c for mean annual temperature). In contrast, regional temperature is positively correlated with TSA, and maximum annual temperature shows the highest correlation (Table 2). Similar with regional temperature TSA shows a long-term linear upward trend, but based on 6th order polynomial regression their correlation is not very clear on a multi-annual periodic time scale (see Fig. 10d for mean annual temperature).

5. Discussion

5.1. Soil salinity dynamics in the Bajestan region and possible regional causes

Soil salinity in the Bajestan region strongly fluctuated between 1992 and 2021 (Figs. 2, 3), and areas with high and very high soil salinity generally increased whereas low saline areas decreased (Fig. 3). Outside the playa basin mainly moderate saline areas, not showing a total net change, were converted to the high and very high salinity classes

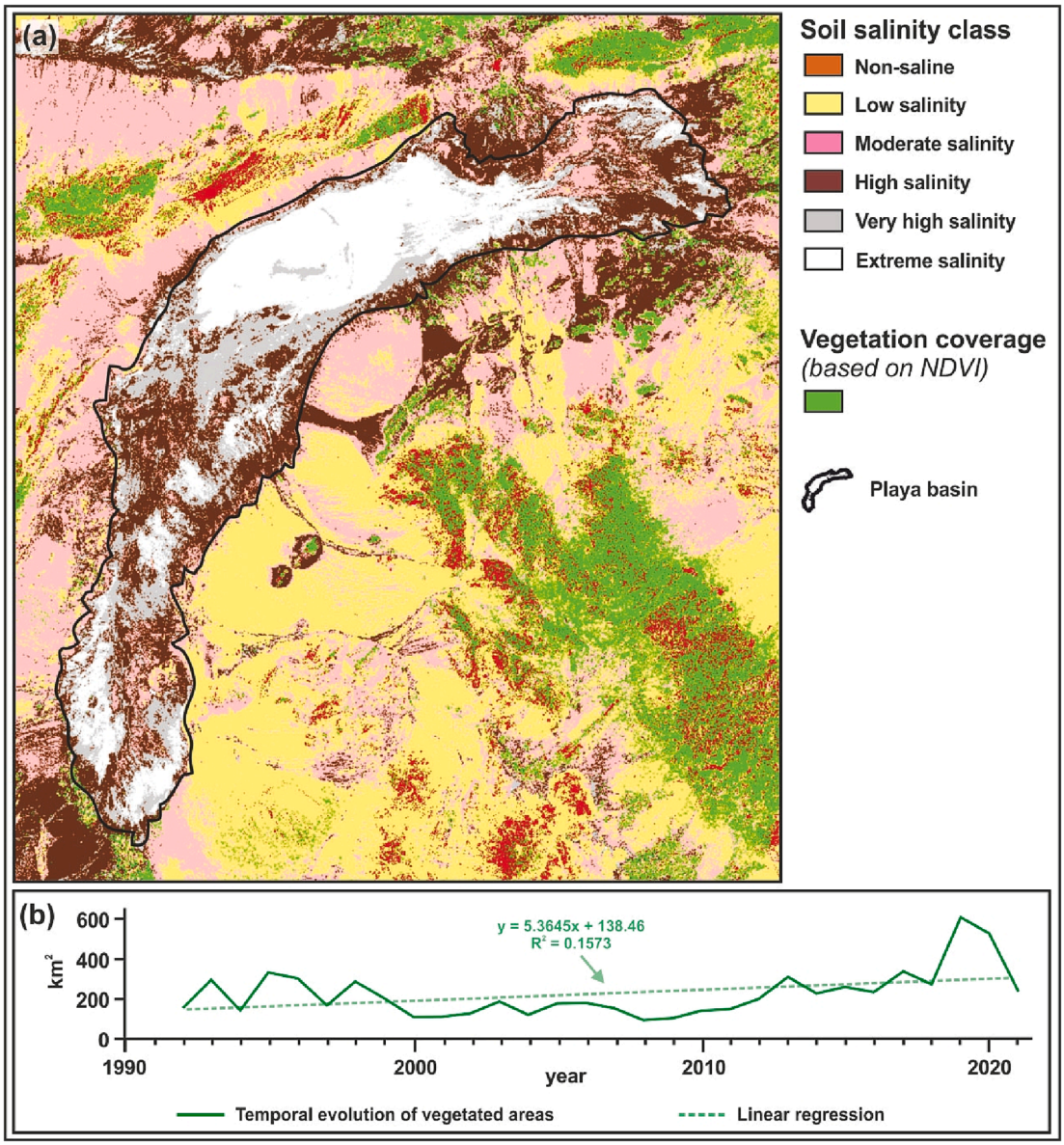

Fig. 5. NDVI-based vegetation density in the study area (vegetated areas show NDVI-values > 0.2) (see Supplementary Table ST-3 for the NDVI values). (a) Map exemplarily showing the extension of the vegetated areas and the six soil salinity classes for May 1992 (this earlier month was chosen for this figure due to a better visibility of the vegetation coverage compared with the NDVI-study period in July). (b) Temporal evolution of the vegetated areas during July.

(Fig. 4a). Hence, this change must have been paralleled by a simultaneous conversion of low saline areas to the moderate class. In contrast, increases of high and very high saline areas within the playa basin occurred mostly at the costs of the extreme class. Conversely, changes towards extreme soil salinity almost exclusively occurred within the playa basin mostly at the costs of very high and high saline areas (Fig. 4b). Hence, our data demonstrate different soil salinity dynamics within and outside the playa basin: Outside the basin, areas of high and very high soil salinity continuously increased over the RS-study period mainly at the costs of low saline areas. Within the basin, areas with high, very high and extreme soil salinity regularly changed into each other (Figs. 2, 4), but without a clear long-term trend (Fig. 3).

The Bajestan region generally became drier (Fig. 6) and warmer (Fig. 7) during the last three decades. However, whereas the drying trend is only recognizable since 1992 but not on the longer climatic time scale since 1961 (Fig. 6), all regional temperature parameters and especially minimum annual temperature distinctly increased since 1961 (Fig. 7). The close relationship between continuously increasing soil salinity, decreasing precipitation and increasing temperature since 1992 is also confirmed by the significant correlations between the merged highest soil salinity classes and regional climatic parameters (Fig. 9, supporting Table ST-4). Hence, similar with former studies (Bannari and Al-Ali, 2020; Rafik et al., 2022) increasing high and very high saline areas outside the playa basin (Fig. 3) are obviously linked with increasing aridity and temperature. Furthermore, there are different time lags between the considered parameters (Fig. 9): Mean annual precipitation positively correlates with a two-year time lag and negatively correlates with a one-year time lag with soil salinity, whereas mean and maximum annual temperature significantly positively correlate with zero time lags. Therefore, high soil salinity in the measurement year can be traced back to higher precipitation two years and low precipitation one year earlier. In contrast, high temperatures increase soil salinity during the same year. The significant positive correlation between the NDVI (vegetation density) and low soil salinity with a zero time lag means that during warmer years both vegetation density and low saline areas decrease, what is also mirrored by the significant

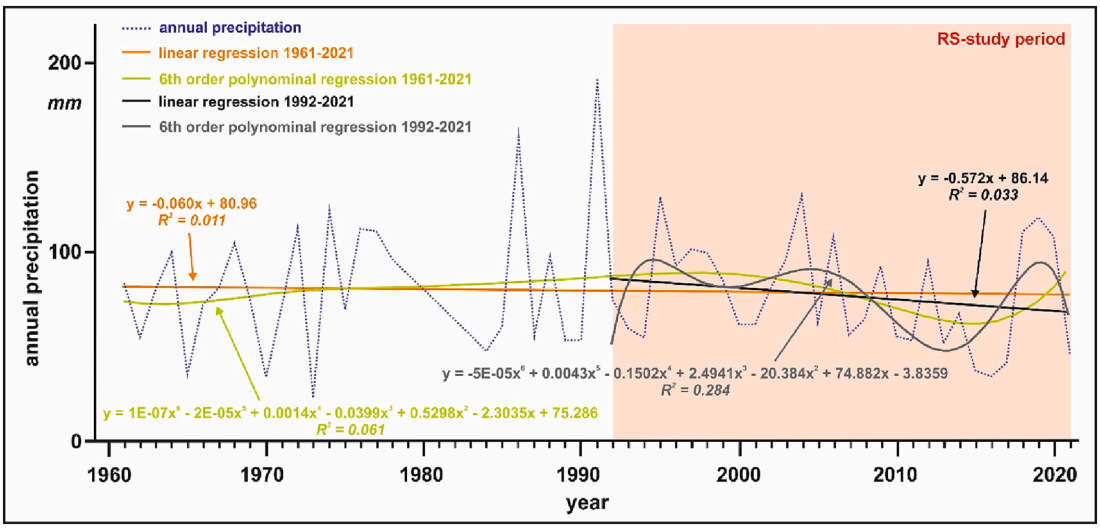

Fig. 6. Mean annual precipitation 1961–2021. Linear and 6th order polynomial regression are separately shown for the long climatic time scale 1961–2021 and the RS-study period 1992–2021.

negative correlation between mean annual temperature and NDVI (Fig. 9). Since most extreme saline areas (during summer) are found within the playa basin (Fig. 2), we cross-correlated this class with the extent of the wet/water-covered area during spring. However, the not significant correlation indicates only a minor effect of wet/water-covered areas on soil salinization in the playa basin.

Summing up, for the areas outside the playa basin showing the largest surfaces with high and very high soil salinity (Fig. 2) we suggest the following causal chain of soil salinization:

(i) During wet years easily soluble salts are leached and mobilized from salt-bearing rocks and sediments into the Bajestan catchment (e.g. from saline lacustrine sediments originating from larger paleolake phases; Behrouzi, 1987; Ashoori et al., 2005; Etikala et al., 2021). While most of these salts are transported by ephemeral tributaries and saline groundwater along the hydraulic gradient into the playa basin, another part still remains in the catchment outside the basin.

(ii) A subsequent dry year then promotes high soil salinity in the catchment, as indicated by the significant negative correlation between soil salinity and precipitation with a time lag of one year. Presumably, salt mobilization and transport still continue with the remaining water from the previous wet year even in this second dry year. However, the moisture is not sufficient to transport large salt amounts further into the playa basin. Therefore, most of the salts remain in the catchment area outside the basin.

(iii) High temperatures during the year of soil salinity measurement lead to increasing evaporation, causing strong surficial salt accumulation due to capillary rise from ground or soil water (Forkutsa et al., 2009; Stavi et al., 2021). In this context, the lower correlation of minimum annual temperature with soil salinity compared with mean and maximum temperature can be explained by the exponential relationship between temperature and evaporation (Gabler et al., 2008). This demonstrates a comparatively lower importance of minimum temperature - mostly measured during night-time - for evaporation. In parallel, vegetation density decreases during such warmer years. Whether this decrease is only caused by increasing evaporation and related lower available soil moisture, or also by increasing soil salinity, cannot be resolved by our data.

The extent of extreme saline areas within the playa basin remained largely continuous since 1992 (Fig. 3), and regular increases and decreases of this class were at the costs of very high and high saline areas and vice versa (Fig. 4b). However, there was an unprecedented strong increase of the extreme saline areas in 2021 (Fig. 3), following an unprecedented three-years wet period 2018–2020 (Fig. 6). Hence, the strong increase of extreme saline areas in 2021 can possibly be explained by an unprecedented intensive transport of easily soluble salts from the catchment into the playa basin during the wet period. This, however, obviously represents an extreme event rather than a trend.

The long-term stability of the non-saline areas since 1992 opposes the general trend of increasing regional soil salinity outside the playa basin, indicating that these areas are little affected by the processes described above. Their unprecedented strong increase in 2021 (Fig. 3) especially in the SE part of our study area (Fig. 2) can thus not be explained so far. However, we hypothesize that strong leaching and transport of easily soluble salts into the playa basin during the preceding 2018 – 2020 wet period could have happened in particular from this SE part of our study area, causing the simultaneous increase of extreme saline areas within the basin. Another explanation could be an enlargement of agricultural activities in the non-saline areas after the wet period, as agricultural use is generally tied to these areas (see Table 1). In addition, a combination of both processes is also conceivable.

Unlike former soil salinity studies that generally used large and irregular time steps or only short sample periods (e.g. Wu et al., 2014; Scudiero et al., 2015; Dasgupta et al., 2015; Bannari and Al-Ali, 2020; Hassani et al., 2020; Rafik et al., 2022; Ma et al., 2023), we analysed soil salinity in the Bajestan region annually over a continuous period of 30 years. Therefore, with this respect we could not only identify long-term soil salinity changes, but also the causal process relationships in detail. Next to the long-term fostering effect of higher temperatures and lower precipitation for increasing soil salinity (Bannari and Al-Ali, 2020; Rafik et al., 2022), we also identified short-term time lags linked with these main controlling factors. Furthermore, unlike many former study areas that were located near coastlines (Dasgupta et al., 2015; Bannari and Al-Ali, 2020) or in intensively irrigated agricultural areas (Wu et al., 2014; Scudiero et al., 2015; Rafik et al., 2022; Ma et al., 2023), our study area is located far away from any coastline and only shows minor human influence. Hence, our detailed results should be representative for the soil salinity dynamics in the vast inland drylands of SW Asia without strong human influence, helping to understand the current and future soil salinity dynamics of these areas. Nevertheless, further factors probably also influenced soil salinity in the Bajestan region or have at

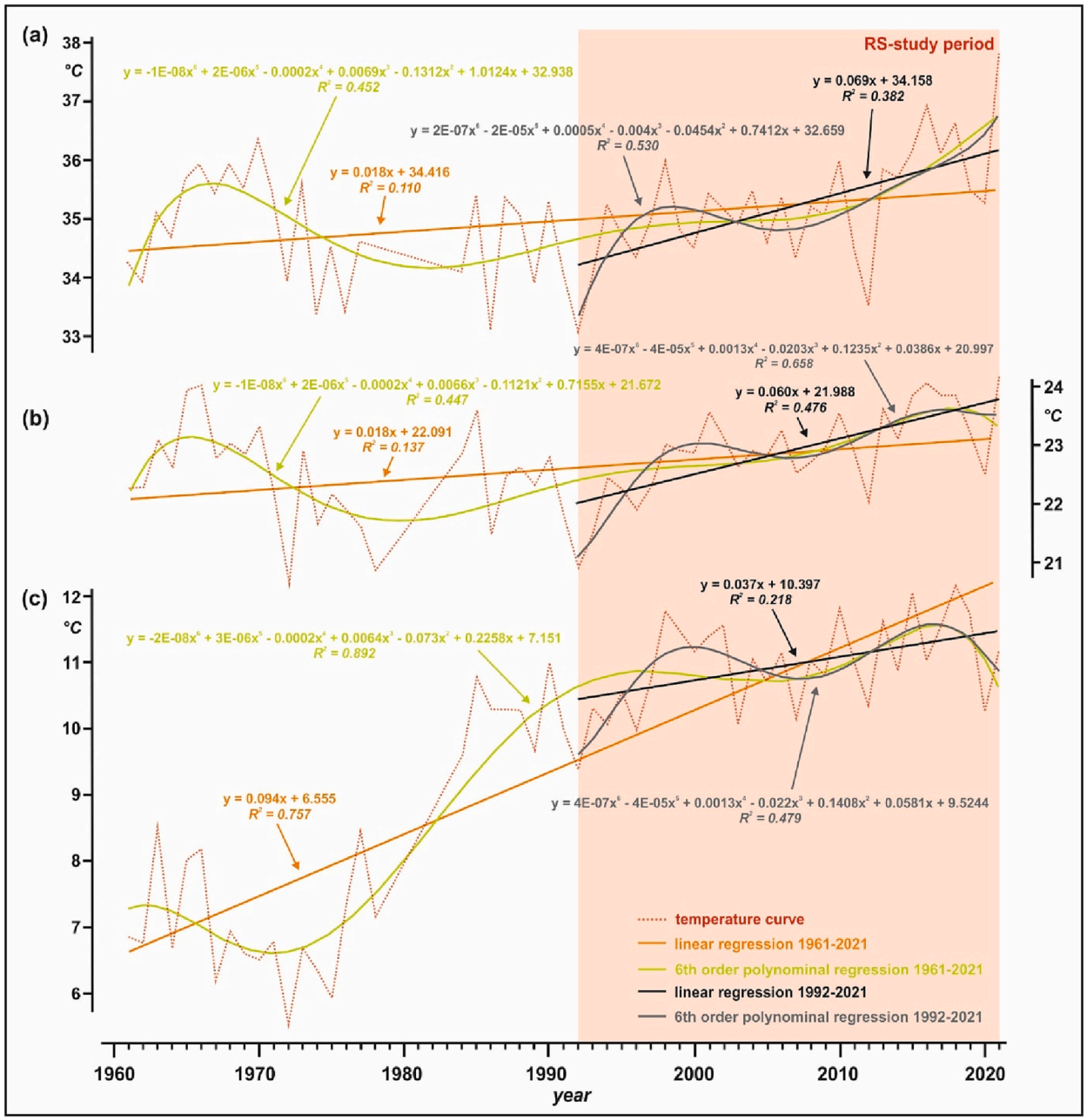

Fig. 7. Temperature changes between 1961 and 2021. Linear and 6th order polynomial regression are separately shown for the long climatic time scale 1961–2021 and the RS-study period 1992–2021. (a) Maximum, (b) average, (c) minimum annual temperature.

least biased our results, such as aeolian activity leading to aeolian removal of salt crusts (Wang et al., 2012) or the regional groundwater dynamics (Wang et al., 2008). Therefore, to quantify these factors further investigations are necessary.

5.2. *Global climatic controls on the soil salinity dynamics in the Bajestan region*

The soil salinity dynamics in the Bajestan region between 1992 and 2021 was mainly controlled by regional precipitation and temperature. Correlation of the latter with different global climate indices showed that regional annual precipitation best correlated with different sub-indices of the global MJO Teleconnection Index (see Table 2). MJO represents a dominant intra-seasonal tropical oscillation, characterized by an eastward zonal shift of the whole pattern of 12,000–20,000 km along the equator within 30–60 days (Madden and Julian, 1971, 1972; Zhang, 2005). It is one of the main factors controlling precipitation in tropical and subtropical regions, widely impacting wind and precipitation patterns in SW-Asia (Iran, Afghanistan, Pakistan) (Barlow et al., 2005; Madhura et al., 2015; Ahmadi et al., 2019). Accordingly, we see a negative relationship between several MJO sub-indices and mean annual precipitation in the Bajestan region, what is also displayed by a completely inverse behavior of mean annual precipitation and the MJO - E70 Index 10 on a multi-annual time scale, i.e. when applying 6th order polynomial regression (Fig. 10a). All regional temperature parameters showed the highest correlations with the global warming GLOTI Index. GLOTI displays global anomalies of Land Surface Air Temperature (LSAT) over land and sea ice and of Sea Surface Temperatures (SSTs) over ice-free water (NASA GISS, 2022). Furthermore, among the considered teleconnection indices POL and TSA show the highest correlations with regional temperature. The negatively correlated POL index, appearing during the cold season, consists of one main polar

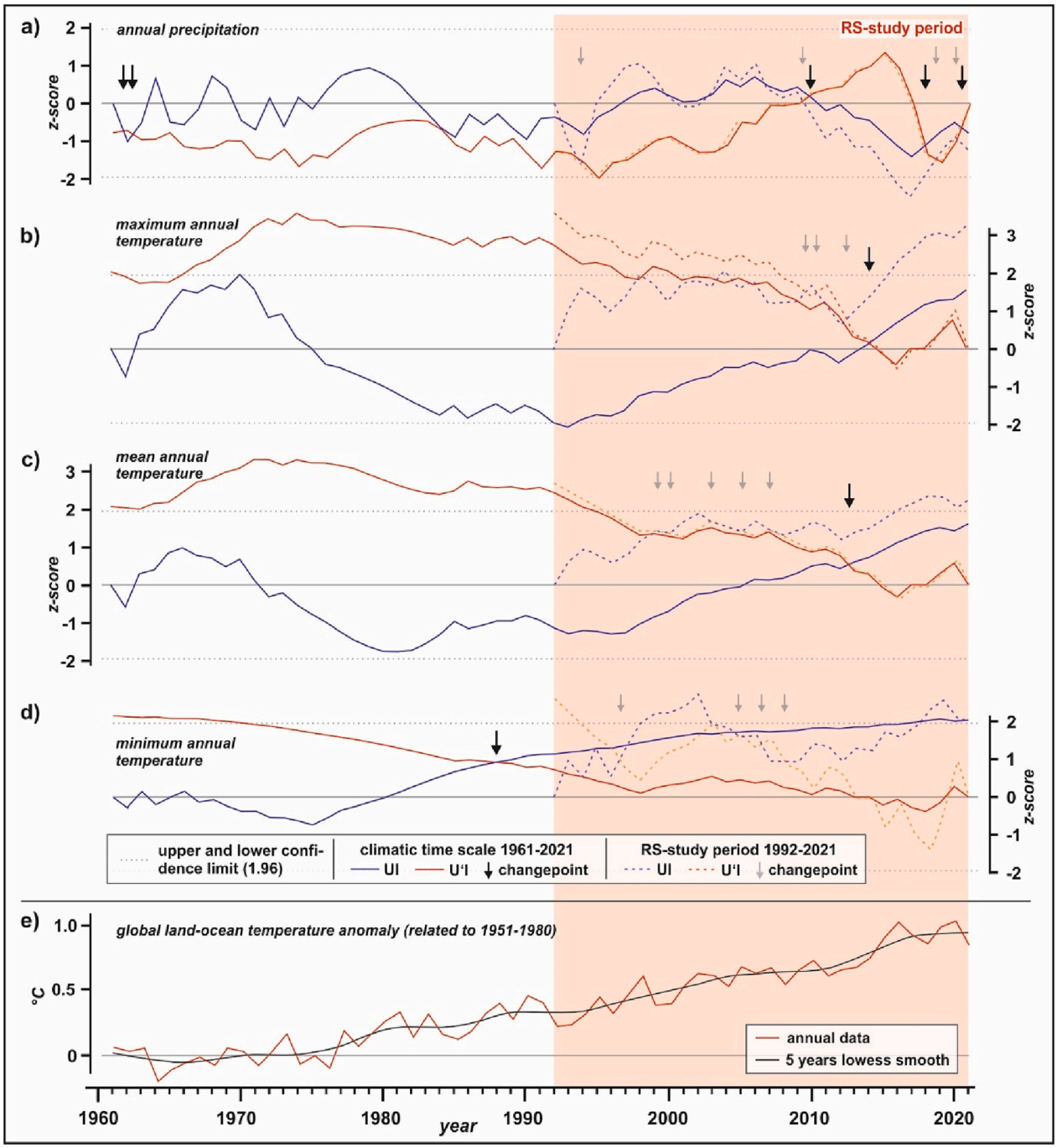

Fig. 8. Mann-Kendall trend analyses for the long climatic time scale 1961–2021 and the shorter RS-study period 1992–2021. (a) mean annual precipitation, (b) maximum annual temperature, (c) mean annual temperature, (d) minimum annual temperature; (e) global land–ocean temperature anomaly related to the period 1951–1980 (https://data.giss.nasa.gov).

anomaly center and separate opposite centers over Europe and NE-China. Thus, it reflects major changes in the strength of the circumpolar circulation by revealing the accompanying systematic mid-latitude circulation changes over large parts of Europe and Asia (Gao et al., 2019). The positively correlated TSA index indicates the SSTs in the Gulf of Guinea between 30°W – 10°E and 20°S – 0° (Enfield et al., 1999).

Summing up, we could identify clear influences of global climatic phenomena on the climate of the Bajestan region. Compared with former studies (Pankova and Konyushkova, 2013; Bannari and Al-Ali, 2020; Okur and Örcen, 2020; Khadimov et al., 2022), this allowed a much deeper look into the linkages between global climate change and regional soil salinization. Whereas mean annual precipitation in the Bajestan region did not show significant systematic changes on the longer time scale since 1961, regional annual temperature was clearly impacted by the global climate change since that time. Due to the location of the Bajestan region in a climatic transitional region, both high and mid-latitude synoptic systems (TSA, POL) play a role in this context. Similar to other regions (Dai, 2011; Ghavidel Rahimi et al., 2017; Sarkar and Maity 2021), we observe the first effects of global warming on the regional climate since the 1970 s. This is particularly evident in the strongly increasing annual minimum temperatures. Mean and maximum annual temperature, on the other hand, were influenced by global warming only during the RS-study period since 1992. This

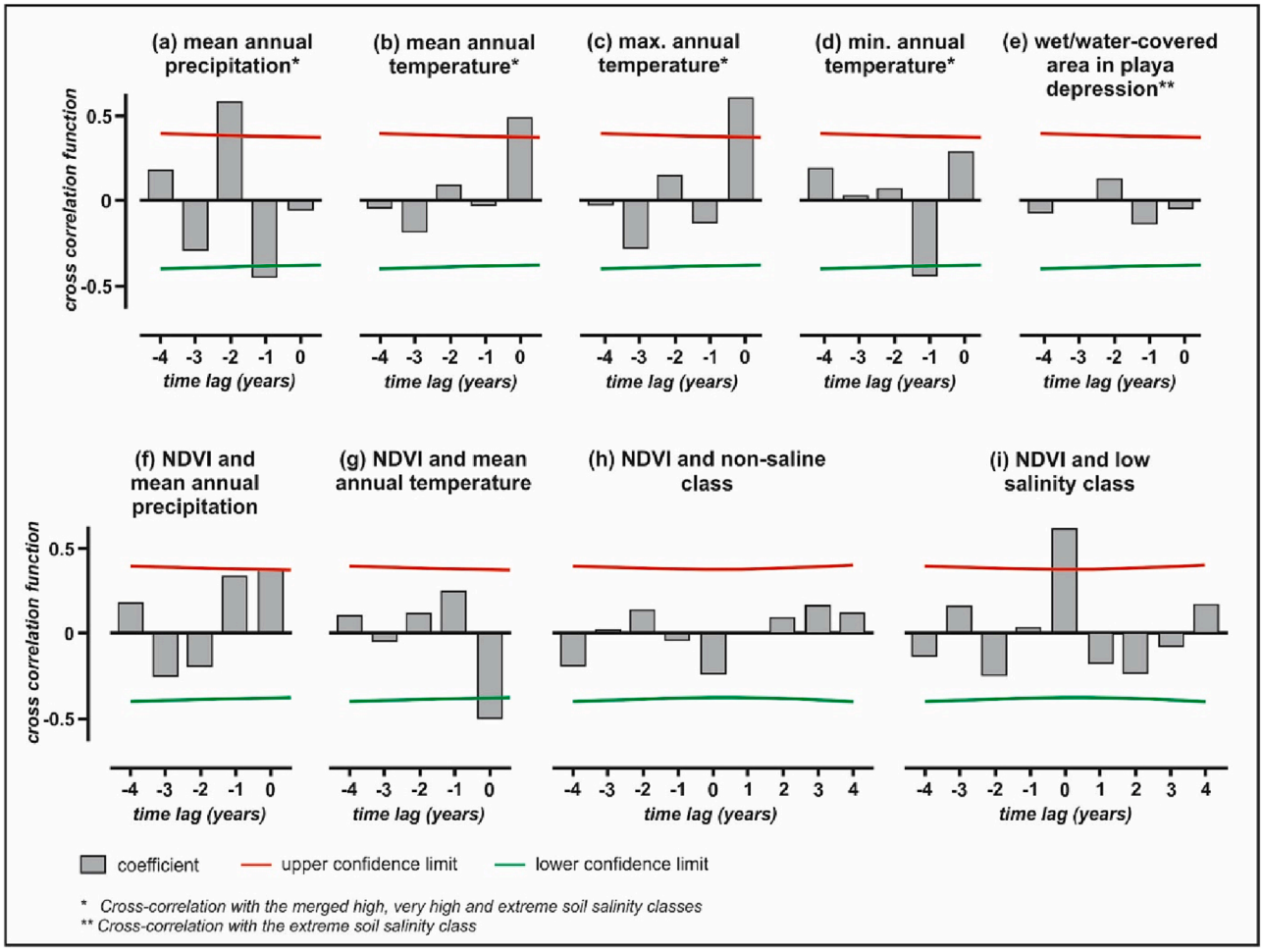

Fig. 9. Graphs of the different cross correlations taking into account possible time lags between soil salinity (merged high, very high and extreme soil salinity classes) and (a) mean annual precipitation, (b) mean annual temperature, (c) maximum annual temperature and (d) minimum annual temperature. Cross correlation between the wet/water-covered area within the playa basin during February/March and extreme soil salinity during July (e). Cross correlation between the NDVI and (f) mean annual precipitation, (g) mean annual temperature, and (h) the non-saline as well as (i) the low soil salinity class. Please note, positive time lags are not possible in reality for the cross-correlations shown in figures (a) – (g), as soil salinity does neither influence regional climate nor the extension of the wet/water-covered area, and patchy dryland vegetation does not significantly influence regional climate.

indicates an intensified regional impact of global warming during the recent years (Figs. 6, 7, 8). Given some influence also of minimum annual temperature on regional soil salinity (Fig. 9), despite missing RS data before 1992 we suspect an influence of global climate change on soil salinity already since the 1970 s. Due to ongoing global warming (Pörtner et al., 2022) probably causing further increasing regional annual temperatures, we also expect a further increase of soil salinization outside the Bajestan playa basin. This will lead to increasing salt dust emissions and increasingly threaten the diverse desert vegetation and wildlife in the regional protected areas. Furthermore, assuming repeated extreme soil salinity conditions within the playa basin such as in 2021, we also expect increasing salt dust emissions from the basin over the coming decades.

6. Conclusions

During this study, we applied a multi-disciplinary research approach encompassing remote sensing, field and laboratory analyses as well as statistical analyses of regional and global climatic parameters to study soil salinity changes and their relation with global climate change in the Bajestan drylands of NE Iran 1992–2021. Thanks to our so far not applied annual time resolution over three decades, we gained much deeper insights into the causal chain of regional soil salinization than during previous studies. Our study shows that both regional annual precipitation and temperature changes control regional soil salinity, but that soil salinity responds to precipitation changes with time lags of up to two years. This probably reflects the time that is needed for the transport of leached soluble salts from their source areas following humid years. In contrast, the reaction of soil salinity to higher temperatures due to increasing capillary rise does not show any time lag. When closer looking into the study area, no systematic changes of extreme soil salinity within the playa basin but just an extreme salinization event in 2021 were observed. In contrast, the areas outside the basin showed a systematic long-term increase of high and very high soil salinity, whereas low saline areas decreased. This was possibly caused by conversions of the moderate to high and very high saline areas, and a parallel increase of the moderate at the costs of low saline areas. Whereas regional annual precipitation did not systematically change during the last six decades, minimum annual temperature increased since the 1970s and mean and maximum annual temperature during the last years. Accordingly, when correlating these regional climate parameters with global climatic indices, the temperature parameters showed the highest correlations with the global warming GLOTI index as well as with the POL and TSA indices being linked with both high- and mid-latitude climatic phenomena, all showing increasing trends during the last years. Given ongoing global climate change, a further increase of

Table 2
Pearson correlations between global climatic indices and annual climate parameters in the Bajestan region. Significant correlations at the 0.95 and 0.99 level are marked with * and **, respectively. Positive correlations are shown in green and negative correlations in red. Furthermore, the highest - positive or negative - correlations of every regional climate parameter with one of the global climatic indices are underlined. (Row 1 to 35 row show teleconnection indices, row 36 the Global Land-Ocean Temperature Anomaly Index (GLOTI), and row 37 the Solar Flux Index).

Row	Global climatic indices	Regional annual precipitation	Regional mean annual temperature	Regional maximum annual temperature	Regional minimum annual temperature
1#	AAO *(Antarctic Osciallation)*	−0.192	**0.470****	**0.597****	**0.497****
2#	AMO *(Atlantic Multidecadal Oscillation)*	0.036	**0.613**	**0.524****	**0.452***
3#	AO (Arctic Oscillation)	−0.151	−0.109	−0.089	−0.190
4#	EA *(East Atlantic Pattern)*	0.298	**−0.564****	**−0.473****	−0.331
5#	EA/WR *(Eastern Asia - Western Russia Pattern)*	0.298	**−0.564****	**−0.473****	−0.331
6#	EP/NP *(East Pacific - North Pacific Oscillation ¯EPO Pattern)*	0.262	**−0.369***	−0.221	−0.191
7#	MEI V2 *(Multivariate ENSO Index)*	0.115	−0.272	−0.133	−0.167
8#	NAO *(North Atlantic Oscillation)*	0.004	−0.108	−0.093	−0.107
9#	NAO-JONES *(North Atlantic Oscillation)*	−0.024	−0.106	−0.172	0.012
10#	NINA 1 + 2 *(Extreme Eastern Tropical Pacific SST)*	0.03	−0.095	0.028	0.108
11#	NINA 3 *(Eastern Tropical Pacific SST)*	0.096	−0.046	0.053	0.087
12#	NINA 4 *(Central Tropical Pacific SST)*	0.174	0.024	0.111	−0.038
13#	NINA 3.4 *(East Central Tropical Pacific SST)*	0.122	−0.075	0.032	−0.024
14#	NP *(North Pacific Pattern)*	0.004	0.227	0.183	0.175
15#	PDO *(Pacific Decadal Oscillation)*	0.047	−0.115	0.040	−0.110
16#	PNA *(Pacific North American Index)*	−0.108	0.027	0.001	0.064
17#	POL *(Polar/Eurasia Pattern)*	0.118	**−0.592****	**−0.526****	**−0.428***
18#	QBO *(Quasi-Biannual Oscillation)*	0.142	0.115	0.149	0.256
19#	SCAN *(Scandinavia Pattern)*	0.057	−0.210	−0.260	−0.064
20#	SOI *(Southern Oscillation Index)*	0.084	0.220	0.130	0.196
21#	TNA *(Tropical Northern Atlantic Index)*	0.016	**0.395***	0.312	0.332
22#	TNI *(Trans Nino Index)*	0.004	0.227	0.183	0.175
23#	TSA *(Tropical Southern Atlantic Index)*	0.053	**0.579****	**0.615****	**0.492****
24#	WHWP *(Western Hemisphere Warm Pool)*	−0.022	**0.441***	**0.482****	**0.421***
25#	WP *(Western Pacific Index)*	−0.123	0.058	0.163	0.079
26#	MJO *(Madden and Julian Oscillation)* - E20 Index 9	**−0.426***	0.259	0.090	−0.002
27#	MJO - E70 Index 10 *(Madden and Julian Oscillation)*	**−0.482****	0.278	0.078	0.034
28#	MJO - E80 Index 1 *(Madden and Julian Oscillation)*	**−0.472****	0.267	0.127	0.023
29#	MJO - E100 Index 2 *(Madden and Julian Oscillation)*	**−0.386***	0.170	0.107	−0.043
30#	MJO - E120 Index 3 *(Madden and Julian Oscillation)*	−0.351	0.162	0.116	−0.071
31#	MJO - E140 Index 4 *(Madden and Julian Oscillation)*	−0.267	0.078	0.127	−0.180
32#	MJO - E160 Index 5 *(Madden and Julian Oscillation)*	−0.171	0.032	0.173	−0.265
33#	MJO - W120 Index 6 *(Madden and Julian Oscillation)*	−0.115	0.032	0.163	−0.245
34#	MJO - W40 Index 7 *(Madden and Julian Oscillation)*	−0.171	0.102	0.121	−0.151
35#	MJO - W10 Index 8 *(Madden and Julian Oscillation)*	−0.308	0.207	0.121	−0.063
36	Global Warming (GLOTI) *(Global Land-Ocean Temperature Anomaly Index)*	−0.111	**0.724****	**0.668****	**0.494****
37	Solar Flux Index *(Solar Flux Cycle Index)*	−0.180	−0.067	−0.248	0.070

#teleconnection index.

soil salinity outside the playa basin should hence be expected. This will have serious consequences for saline dust emissions and the diverse desert vegetation and wildlife in the regional protected areas, and saline dust emissions could furthermore be reinforced by extreme salinity events within the playa depression as that in 2021. This will possibly also increase the number of climatic refugees from the affected regions during the coming decades. Altogether, our multi-disciplinary approach shows a high potential for future applications also in other salinity-affected drylands, making it a pioneer study for research on soil salinization in the context of global warming as a base for the planning of effective strategies in combatting dryland degradation and to forecast the aeolian dust dynamics.

Funding

This research received no external funding.

CRediT authorship contribution statement

Azra Khosravichenar: Conceptualization, Methodology, Software, Formal analysis, Investigation, Writing – original draft, Writing – review & editing, Visualization. **Mehdi Aalijahan:** Conceptualization, Methodology, Software, Formal analysis, Investigation, Writing – original draft, Writing – review & editing, Visualization. **Saeid Moaazeni:** . **Anthony R. Lupo:** Writing – review & editing. **Alireza Karimi:** Writing – review & editing. **Mathias Ulrich:** Writing – review & editing. **Naser Parvian:** . **Aboozar Sadeghi:** . **Hans von Suchodoletz:** Conceptualization, Investigation, Writing – original draft, Writing – review & editing.

Declaration of Competing Interest

The authors declare that they have no known competing financial interests or personal relationships that could have appeared to influence

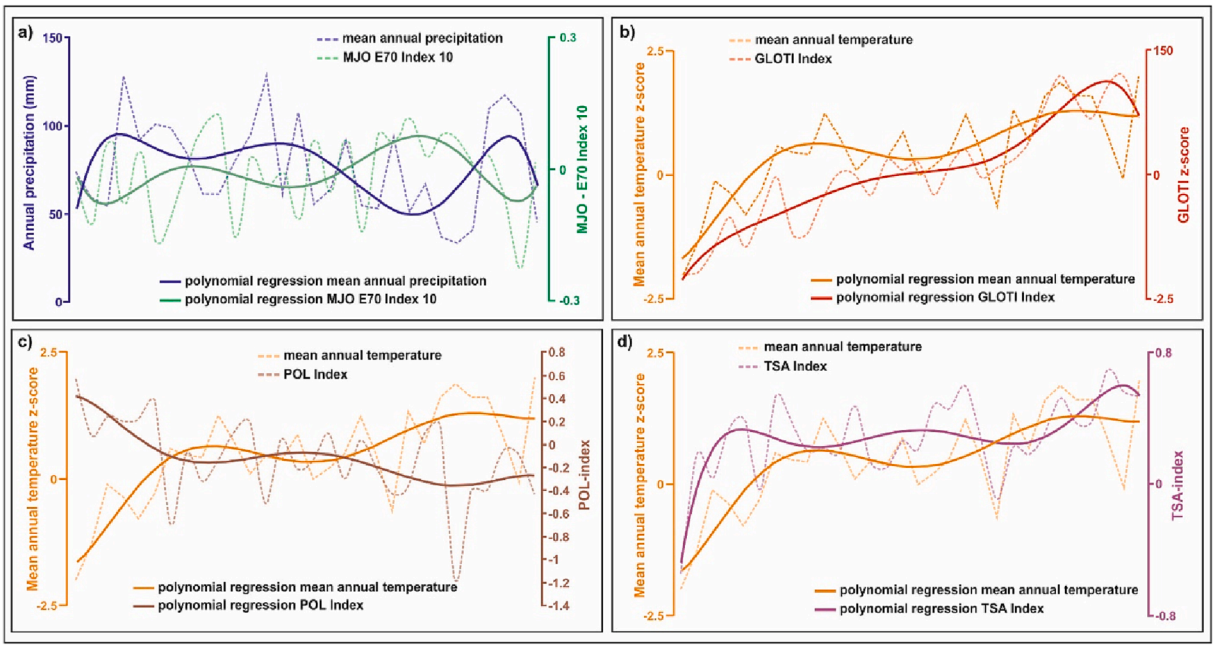

Fig. 10. 6th order polynomial relationships between annual climate parameters of the Bajestan region and global climatic indices showing the highest correlations for the RS-study period 1992 – 2021: (a) MJO - E70 Index 10 and mean annual precipitation, (b) Global Land-Ocean Temperature Anomaly Index (GLOTI Index) and mean annual temperature, c) POL Index and mean annual temperature, d) TSA Index and mean annual temperature.

the work reported in this paper.

Data availability

Data will be made available on request.

Acknowledgments

The authors would like to thank the Iranian Meteorological Organization and the NOAA Organization for providing access to meteorological data from the Bajestan region stations and Global climate indexes. The authors acknowledge the role of the anonymous reviewers and the editor-in-chief who helped strengthen this work. The authors wish to express their gratitude to the Leipzig and Dresden University authorities for generously covering the publication fee for this paper.

Appendix A. Supplementary data

Supplementary data to this article can be found online at https://doi.org/10.1016/j.ecolind.2023.110639.

References

Aalijahan, M., Karataş, A., Lupo, A.R., Efe, B., Khosravichenar, A., 2023. Analyzing and modeling the spatial-temporal changes and the impact of GLOTI Index on precipitation in the Marmara region of Türkiye. Atmosphere-Basel 14, 489.
Aalijahan, M., Khosravichenar, A., 2021. A multimethod analysis for average annual precipitation mapping in the Khorasan Razavi Province (Northeastern Iran). Atmosphere-Basel 12, 592.
Aalijahan, M., Salahi, B., Rahimi, Y.G., Asl, M.F., 2019. A new approach in temporal-spatial reconstruction and synoptic analysis of cold waves in the northwest of Iran. Theor. Appl. Climatol. 137 (1-2), 341–352.
Aalijahan, M., Lupo, A.R., Salahi, B., Rahimi, Y.G., Asl, M.F., 2022. The long-term (142 years) spatiotemporal reconstruction and synoptic analysis of extreme low temperatures (− 15° C or lower) in the northwest region of Iran. Theor. Appl. Climatol. 147, 1415–1436.
Ahmadi, M., Salimi, S., Hosseini, S.A., Poorantiyosh, H., Bayat, A., 2019. Iran's precipitation analysis using synoptic modeling of major teleconnection forces (MTF). Dynam. Atmos. Oceans 85, 41–56.
Ahmadirouhani, R., Rahimi, B., Karimpour, M.H., Shafaroudi, A.M., Najafi, S.A., Pour, A. B., 2017. Fracture mapping of lineaments and recognizing their tectonic significance using SPOT-5 satellite data: A case study from the Bajestan area, Lut Block, east of Iran. J. Afr. Earth Sc. 134, 600–612.
Alijani, B., Harman, J.R., 1985. Synoptic climatology of precipitation in Iran. Ann. Assoc. Am. Geogr. 75 (3), 404–416.
Alizadeh-Choobari, O., Zawar-Reza, P., Sturman, A., 2014. The "wind of 120 days" and dust storm activity over the Sistan Basin. Atmos. Res. 143, 328–341.
Ashoori, A. R., Karimpour, M.H., Saadat, S., 2005. Geological map of Bajestan. scale: 1: 10000. Geological Survey of Iran.
Bannari, A., Al-Ali, Z.M., 2020. Assessing climate change impact on soil salinity dynamics between 1987–2017 in arid landscape using Landsat TM, ETM+ and OLI data. Remote Sens.-Basel 12, 2794.
Barlow, M., Wheeler, M., Lyon, B., Cullen, H., 2005. Modulation of daily precipitation over southwest Asia by the Madden-Julian oscillation. Mon. Weather Rev. 133, 3579–3594.
Begum, B., Tajbar, S., Khan, B., Rafiq, L., 2021. Identification of relationships between climate indices and precipitation fluctuation in Peshawar City-Pakistan. J. Res. Environ. Earth Sci. 10, 264–278.
Behrouzi A., 1987. Feiz-Abad geology map, 1: 100000 scale. National Geological Organization of Iran.
Benedict, Jaelani, L.M., 2021. A long-term spatial and temporal analysis of NDVI changes in Java Island using Google Earth Engine. IOP C. Ser. Earth Env. 936 (1), 012038.
Bowen, M.W., Johnson, W.C., 2017. Anthropogenically accelerated sediment accumulation within playa wetlands as a result of land cover change on the High Plains of the central United States. Geomorphology 294, 135–145.
Briere, P.R., 2000. Playa, playa lake, sabkha: Proposed definitions for old terms. J. Arid Environ. 45 (1), 1–7.
Burrell, A.L., Evans, J.P., de Kauwe, M.G., 2020. Anthropogenic climate change has driven over 5 million km^2 of drylands towards desertification. Nat. Commun. 11, 3853.
Cetin, M., Isik Pekkan, O., Bilge Ozturk, G., Senyel Kurkcuoglu, M.A., Kucukpehlivan, T., Cabuk, A., 2022. Examination of the change in the vegetation around the Kirka Boron mine site by using remote sensing techniques. Water Air Soil Poll. 233, 254.
Chen, J., Yang, S., Li, H., Zhang, B., Lv, J., 2013. Research on geographical environment unit division based on the method of natural breaks (Jenks). Int. Arch. Photogramm. Remote. Sens. Spat. Inf. Sci. 3, 47–50.
Cicek, N., Erdogan, M., Yucedag, C., Cetin, M., 2022. Improving the detrimental aspects of salinity in salinized soils of arid and semi-arid areas for effects of vermicompost leachate on salt stress in seedlings. Water Air Soil Poll. 233, 197.
Dai, A., 2011. Drought under global warming: a review. Clim. Change 2 (1), 45–65.
Dasgupta, S., Hossain, M.M., Huq, M., Wheeler, D., 2015. Climate change and soil salinity: The case of coastal Bangladesh. Ambio 44 (8), 815–826.
Davis, J.C., Sampson, R.J., 1986. Statistics and data analysis in geology, Vol. 646. Wiley, New York.
Dehaan, R.L., Taylor, G.R., 2002. Field-derived spectra of salinized soils and vegetation as indicators of irrigation-induced soil salinization. Remote Sens. Environ. 80 (3), 406–417.
Dewan, M.L., Famouri, J., 1961. Soil map of Iran. FAO, Tehran.
Eastman, J.R., He, J., 2020. A regression-based procedure for Markov transition probability estimation in land change modeling. Land 9, 407.
Ebrahimzadeh, I., Esmaeil Negad, M., 2017. The future challenge of climatic refugees regional developments. Case study: South Khorasan. Geography and Development 15, 1–18.

Emadodin, I., Reinsch, T., Taube, F., 2019. Drought and Desertification in Iran. Drought and desertification in Iran. Hydrology 6 (3), 66.
Enfield, D.B., Mestas-Nuñez, A.M., Mayer, D.A., Cid-Serrano, L., 1999. How ubiquitous is the dipole relationship in tropical Atlantic Sea surface temperatures? J. Geophys. Res.-Oceans 104 (C4), 7841–7848.
Etikala, B., Adimalla, N., Madhav, S., Somagouni, S.G., Keshava Kiran Kumar, P.L., 2021. Salinity problems in groundwater and management strategies in arid and semi-arid regions. In: Madhav, S., Singh, P. (Eds.), Groundwater Geochemistry: Pollution and Remediation Methods. Wiley & Sons, Chichester, pp. 42–56.
Feng, S., Fu, Q., 2013. Expansion of global drylands under a warming climate. Atmos. Chem. Phys. 13, 10081–10094.
Feyisa, G.L., Meilby, H., Fensholt, R., Proud, S.R., 2014. Automated Water Extraction Index: A new technique for surface water mapping using Landsat imagery. Remote Sens. Environ. 140, 23–35.
Forkutsa, I., Sommer, R., Shirokova, Y.I., Lamers, J.P.A., Kienzler, K., Tischbein, B., Martius, C., Vlek, P.L.G., 2009. Modeling irrigated cotton with shallow groundwater in the Aral Sea Basin of Uzbekistan: II. Soil salinity dynamics. Irrigation Sci. 27 (4), 319–330.
Gabler, R.E., Petersen, J.F., Trapasso, L.M., Sack, D., 2008. Physical Geography. Cengage Learning.
Gao, N.i., Bueh, C., Xie, Z., Gong, Y., 2019. A novel identification of the Polar/Eurasia pattern and its weather impact in May. J. Meteorol. Res.-PRC. 33 (5), 810–825.
Ge, Y., Abuduwaili, J., Ma, L., Altausen, D., Abdullaev, S., Hofer, J., 2019. Lakes in arid land and saline dust storms. E3S Web of Conferences 99, 01007.
Ghavidel Rahimi, Y., Farajzadeh, M., Aalijahan, M., 2017. The assessment of Iran monthly and seasonal mean temperatures sensitivity to global land-oceans mean temperature index. Journal of Geographical Space 17, 25–47 in Persian.
Guilmoto, C., Oliveau, S., 2018. Population distribution across Asia. In: Routledge Handbook of Asian Demography. Routledge, pp. 268–284.
Hassani, A., Azapagic, A., Shokri, N., 2020. Predicting long-term dynamics of soil salinity and sodicity on a global scale. PNAS 117 (52), 33017–33027.
Hou, J., Rusuli, Y., 2022. Assessment of soil salinization risk by Remote Sensing-based Ecological Index (RSEI) in the Bosten Lake watershed, Xinjiang in northwest China. Sustainability 14, 7118.
Huang, J., Li, Y., Fu, C., Chen, F., Fu, Q., Dai, A., Shinoda, M., Ma, Z., Guo, W., Li, Z., Zhang, L., Liu, Y., Yu, H., He, Y., Xie, Y., Guan, X., Ji, M., Lin, L., Wang, S., Yan, H., Wang, G., 2017. Dryland climate change: Recent progress and challenges. Rev. Geophys. 55 (3), 719–778.
Khadimov, M., Ishchanov, J., Hamidov, A., Donmez, C., Djumaboev, K., 2022. Assessment of soil salinity changes under the climate change in the Khorezm region, Uzbekistan. Int. J. Env. Res. Pub. He. 19, 8794.
Khan, N.M., Rastoskuev, V.V., Sato, Y., Shiozawa, S., 2005. Assessment of hydrosaline land degradation by using a simple approach of remote sensing indicators. Agr. Water Manage. 77 (1-3), 96–109.
Khosravi, A., Asghari lafamjani, S., Alipour, M., 2014. Applying fuzzy logic in optimized rural site selection and analysis of current location of the villages in proportion to natural factors (central desert in the study area of Bardaskan). Applied Geomorphology of Iran 2 (4), 78–89.
Khosravichenar, A., Fattahi, M., Amini, H., Suchodoletz, H.V., 2020. The potential of small mountain river systems for paleoenvironmental reconstructions in drylands—an example from the Binaloud Mountains in northeastern Iran. Geosciences 10 (11), 448.
Khosravichenar, A., Fattahi, M., Karimi, A., Fazeli Nashli, H., von Suchodoletz, H., 2021. A first outline of the Quaternary landscape evolution of the Kashaf Rud River basin in the drylands of northeastern Iran. E&G Quaternary Science Journal 70 (1), 145–150.
Krinsley, D.B., 1970. A Geomorphological and Paleoclimatological Study of the Playas of Iran. Part II. Geological Survey, Reston VA.
Kweku, D.W., Bismark, O., Maxwell, A., Desmond, K.A., Danso, K.B., Oti-Mensah, E.A., Quachie, A.T., Adormaa, B.B., 2018. Greenhouse effect: Greenhouse gases and their impact on global warming. J. Sci. Res. Rep. 17, 1–9.
Lanzante, J.R., 1996. Resistant, robust and non-parametric techniques for the analysis of climate data: Theory and examples, including applications to historical radiosonde station data. Int. J. Climatol. 16 (11), 1197–1226.
Liu, D., Abuduwaili, J., Wang, L., 2015. Salt dust storm in the Ebinur Lake region: its 50-year dynamic changes and response to climate changes and human activities. Nat. Hazards 77 (2), 1069–1080.
Liu, J., Xue, B., A, Y., Sun, W., Guo, Q., 2020. Water balance changes in response to climate change in the upper Hailar River Basin. China. Hydrol. Res. 51 (5), 1023–1035.
Ma, S., He, B., Xie, B., Ge, X., Han, L., 2023. Investigation of the spatial and temporal variation of soil salinity using Google Earth Engine: a case study at Werigan-Kuqa Oasis, West China. Sci. Rep.-UK 13, 2754.
Madden, R.A., Julian, P.R., 1971. Detection of a 40–50-day oscillation in the zonal wind in the tropical Pacific. J. Atmos. Sci. 28 (5), 702–708.
Madden, R.A., Julian, P.R., 1972. Description of global-scale circulation cells in the tropics with a 40–50-day period. J. Atmos. Sci. 29 (6), 1109–1123.
Madhura, R.K., Krishnan, R., Revadekar, J.V., Mujumdar, M., Goswami, B.N., 2015. Changes in western disturbances over the Western Himalayas in a warming environment. Clim. Dynam. 44 (3-4), 1157–1168.
Menke, W., Menke, J., 2016. Environmental data analysis with Matlab. In: Environmental Data Analysis With Matlab. Elsevier, pp. 1–19.
Metternicht, G.I., Zinck, J.A., 2003. Remote sensing of soil salinity: potentials and constraints. Remote Sens. Environ. 85 (1), 1–20.
Metternicht, G., Zinck, A., 2008. Remote sensing of soil salinization: Impact on land management. CRC Press, Boca Raton, FL.
Mianabadi, A., Davary, K., Kolahi, M., Fisher, J., 2022. Water/climate nexus environmental rural-urban migration and coping strategies. J. Environ. Plann. Man. 65 (5), 852–876.
Middleton, N.J., 1986. A geography of dust storms over southwest Asia. J. Climatol. 6, 183–196.
Montgomery, D.C., Peck, E.A., Vining, G.G., 2021. Introduction to linear regression analysis. John Wiley & Sons.
Nama, A.H., Abbas, A.S., Maatooq, J.S., 2022. Field and satellite images-based investigation of rivers morphological aspects. Civil Engineering Journal 8, 1339–1357.
NASA GISS, 2022. GISS Surface Temperature Analysis (GISTEMP v4) Frequently Asked Questions (https://data.giss.nasa.gov/gistemp/faq/).
National Iranian Oil Company, 1957. Geological map of Iran 1 : 2.500000. Orell Füssli, Zürich.
Nawar, S., Buddenbaum, H., Hill, J., 2015. Digital mapping of soil properties using multivariate statistical analysis and ASTER data in an arid region. Remote Sens.-Basel 7, 1181–1205.
Noroozi, J., Talebi, A., Doostmohammadi, M., Manafzadeh, S., Asgarpour, Z., Schneeweiss, G.M., 2019. Endemic diversity and distribution of the Iranian vascular flora across phytogeographical regions, biodiversity hotspots and areas of endemism. Sci. Rep.-UK 9, 12991.
Oktaviani, F., Miftahuddin, Setiawan, I., 2021. Cross-correlation analysis between sea surface temperature anomalies and several climate elements in the Indian Ocean. Parameter: Journal of. Statistics 1 (1), 13–20.
Okur, B., Örcen, N., 2020. Chapter 12 - Soil salinization and climate change. In: Vara Prasad, M.N., Pietrzykowski, M. (Eds.), Climate Change and Soil Interactions. Elsevier, Amsterdam, pp. 331–350.
Pankova, Y.I., Konyushkova, M.V., 2013. Effect of global warming on soil salinity of the arid regions. Russ. Agric. Sci. 39 (5-6), 464–467.
Perri, S., Suweis, S., Entekhabi, D., Molini, A., 2018. Vegetation controls on dryland salinity. Geophys. Res. Lett. 45 (21), 11,669–11,682.
Pohlert, T., 2016. Non-parametric trend tests and change-point detection. https://cran.microsoft.com/snapshot/2017-11-08/web/packages/trend/vignettes/trend.pdf.
Pörtner, H.O., Roberts, D.C., Adams, H., Adler, C., Aldunce, P., Ali, E., Ibrahim, Z.Z., 2022. Climate change 2022: Impacts, adaptation and vulnerability. IPCC, Geneva, Switzerland, p. 3056.
Rafik, A., Ibouh, H., El Alaoui El Fels, A., Eddahby, L., Mezzane, D., Bousfoul, M., Amazirh, A., Ouhamdouch, S., Bahir, M., Gourf, A., Dhiba, D., Chehbouni, A., 2022. Soil salinity detection and mapping in an environment under water stress between 1984 and 2018 (Case of the largest oasis in Africa-Morocco). Remote Sens.-Bsael 14, 1606.
Ravi, S., Breshears, D.D., Huxman, T.E., D'Odorico, P., 2010. Land degradation in drylands: Interactions among hydrologic-aeolian erosion and vegetation dynamics. Geomorphology 116 (3-4), 236–245.
Rengasamy, P., 2006. World salinization with emphasis on Australia. J. Exp. Bot. 57, 1017–1023.
Rossi, R.E., Mulla, D.J., Journel, A.G., Franz, E.H., 1992. Geostatistical tools for modeling and interpreting ecological spatial dependence. Ecol. Monogr. 62 (2), 277–314.
Sarkar, S., Maity, R., 2021. Global climate shift in 1970s causes a significant worldwide increase in precipitation extremes. Sci. Rep.-UK 11, 11574.
Sayari, N., Bannayan, M., Alizadeh, A., Farid, A., 2013. Using drought indices to assess climate change impacts on drought conditions in the northeast of Iran (case study: Kashafrood basin). Meteorol. Appl. 20 (1), 115–127.
Scudiero, E., Skaggs, T.H., Corwin, D.L., 2015. Regional-scale soil salinity assessment using Landsat ETM+ canopy reflectance. Remote Sens. Environ. 169, 335–343.
Shaw, R.J., 1994. Estimation of the electrical conductivity of saturation extracts from the electrical conductivity of 1: 5 soil: water suspensions and various soil properties. Project Report Series QO94025. Department of Primary Industries, Queensland, Australia.
Sokhanvar, F., Ejtehadi, H., Vaezi, J., Memariani, F., Joharchi, M.R., Ranjbar, Z., 2013. Flora, life form and chorology of plants of the Helali protected area in Khorasan-e Razavi province. Taxonomy and Biosystematics 5, 85–100.
Stavi, I., Thevs, N., Priori, S., 2021. Soil salinity and sodicity in drylands: A review of causes, effects, monitoring, and restoration measures. Front. Environ. Sci. 9 https://doi.org/10.3389/fenvs.2021.712831.
Stockle, C.O., 2002. Environmental impact of irrigation: A review. https://citeseerx.ist.psu.edu/viewdoc/download?doi=10.1.1.488.4861&rep=rep1&type=pdf.
Sung, J.H., Chung, E.-S., Kim, Y., Lee, B.-R., 2017. Meteorological hazard assessment based on trends and abrupt changes in rainfall characteristics on the Korean peninsula. Theor. Appl. Climatol. 127 (1-2), 305–326.
Szabó, S., Gácsi, Z., Balázs, B., 2016. Specific features of NDVI, NDWI and MNDWI as reflected in land cover categories. Acta Geographica Debrecina, Landscape & Environment Series 10 (3-4), 194–202.
Thiam, S., Villamor, G.B., Faye, L.C., Sène, J.H.B., Diwediga, B., Kyei-Baffour, N., 2021. Monitoring land use and soil salinity changes in coastal landscape: a case study from Senegal. Environ. Monit. Assess. 193, 1–18.
Torshizian, H., Mousavi Harami, S.R., 1999. Geomorphological analysis of Bajestan playa and its surrounding area in northeast Iran. Geographical Researches 52, 219–240 in Persian.
Tucker, C.J., 1979. Red and photographic infrared linear combinations for monitoring vegetation. Remote Sens. Environ. 8 (2), 127–150.
Ullmann, T., Serfas, K., Büdel, C., Padashi, M., Baumhauer, R., 2019. Data Processing, feature extraction, and time-series analysis of Sentinel-1 Synthetic Aperture Radar (SAR) imagery: examples from Damghan and Bajestan Playa (Iran). Z. Geomorph. 62 (1), 9–39.

UNEP-WCMC, 2007. A spatial analysis approach to the global delineation of dryland areas of relevance to the CBD programme of work on dry and subhumid lands. Cambridge, UK.
Wang, X., Hua, T., Zhang, C., Lang, L., Wang, H., 2012. Aeolian salts in Gobi deserts of the western region of Inner Mongolia: Gone with the dust aerosols. Atmos. Res. 118, 1–9.
Wang, Y., Xiao, D., Li, Y., Li, X., 2008. Soil salinity evolution and its relationship with dynamics of groundwater in the oasis of inland river basins: case study from the Fubei region of Xinjiang Province. China. Environ. Monit. Assess. 140 (1-3), 291–302.
Wang, X., Xiao, X., Zou, Z., Hou, L., Qin, Y., Dong, J., Doughty, R.B., Chen, B., Zhang, X. i., Chen, Y., Ma, J., Zhao, B., Li, B.o., 2020. Mapping coastal wetlands of China using time series Landsat images in 2018 and Google Earth Engine. ISPRS J. Photogramm. 163, 312–326.
Wu, W., Mhaimeed, A.S., Al-Shafie, W.M., Ziadat, F., Dhehibi, B., Nangia, V., de Pauw, E., 2014. Mapping soil salinity changes using remote sensing in Central Iraq. Geoderma Reg. 2 (3), 21–31.
Yadav, R., Tripathi, S.K., Pranuthi, G., Dubey, S.K., 2014. Trend analysis by Mann-Kendall test for precipitation and temperature for thirteen districts of Uttarakhand. J. Agrometeorol. 16, 164.
Ye, X., Zhang, Q., Liu, J., Li, X., Xu, C.Y., 2013. Distinguishing the relative impacts of climate change and human activities on variation of streamflow in the Poyang Lake catchment. China. Journal Hydrol. 494, 83–95.
Zeren Cetin, I., Varol, T., Ozel, H.B., Sevik, H., 2023. The effects of climate on land use/cover: a case study in Turkey by using remote sensing data. Environ. Sci. Pollut. R. 30 (3), 5688–5699.
Zhang, C., 2005. Madden-Julian Oscillation. Rev. Geophys. 43, RG2003.
Zhang, X., Li, P., Li, D., 2018. Spatiotemporal variations of precipitation in the southern part of the Heihe river basin (China), 1984–2014. Water 10, 410.
Zucca, C., Middleton, N., Kang, U., Liniger, H., 2021. Shrinking water bodies as hotspots of sand and dust storms: The role of land degradation and sustainable soil and water management. Catena 207, 105669.

Websites and Data sources:

Local Meteorological data sources: Iran meteorological organization (https://www.irimo.ir/).
Digital Elevation Model GTOPO30. (https://earthexplorer.usgs.gov).
Stream wind data. (https://psl.noaa.gov/data/gridded/data.ncep.reanalysis.html).
Landsat imagery data: USGS. (https://earthexplorer.usgs.gov/).
ESRI 2019. (https://www.esri.com/en-us/home).